IRF Uppsala

Seminar 6 November 2013

Schumann resonances in the Earth-ionosphere cavity

by Sergio Toledo Redondo

Outline

1. Introduction

1. The Earth-ionosphere cavity
2. Lightning as the main source of Schumann resonances
3. Seismo-electromagnetism

2. Numerical simulations

1. Lossless and lossy cavities
2. Earthquake precursors
3. Effect of the day-night asymmetry

3. Measurements and observations

1. Schumann resonances from Magnetotelluric records
2. Schumann resonance station in Sierra Nevada, Spain
3. Detection from space
4. Cut-off frequency of the Earth-ionosphere waveguide

4. Present and future in Schumann resonance studies

The Earth-ionosphere cavity

On a global scale, the **Earth** can be considered as a **conducting sphere surrounded by air**. However, at around 40–50 km of height from the surface, the **lower ionosphere** becomes increasingly **conductive**. This structure forms an electromagnetic cavity with its own **resonant modes** in the ELF (**Schumann resonances**) and ULF (**atmospherics**) ranges. This cavity can accommodate two kinds of standing waves: the transverse electric (TEr) and the transverse magnetic (TMr) to the radial direction modes.

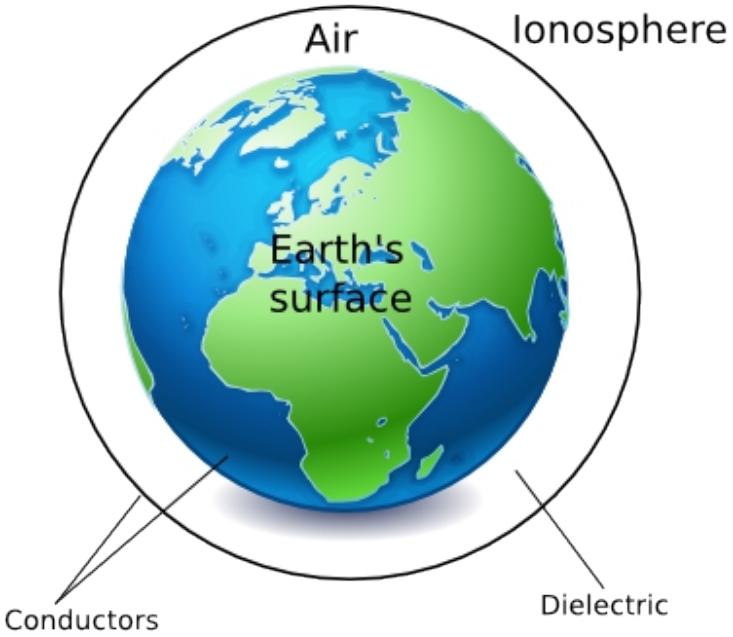

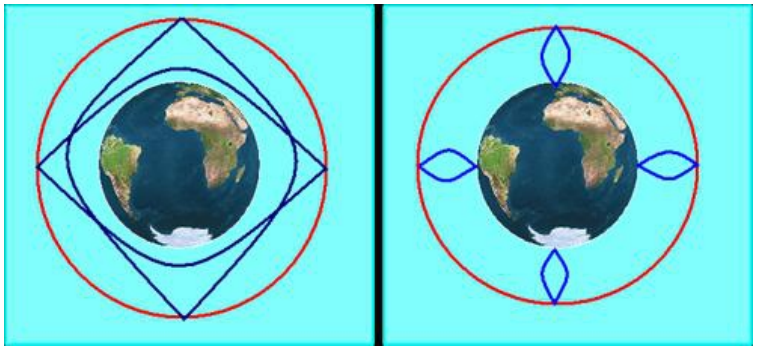

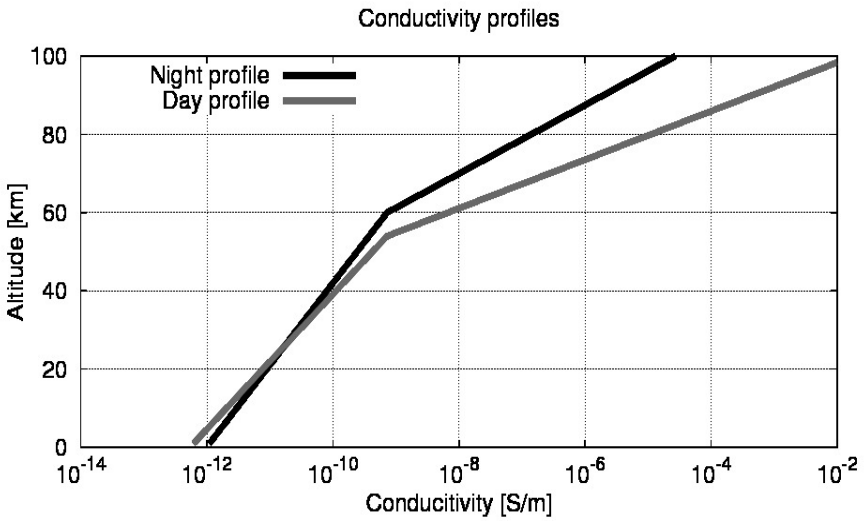

Nickolaenko, A. P., and M. Hayakawa, *Resonances in the Earth - Ionosphere Cavity,* Kluwer Acad., Dordrecht, The Netherlands, 2002.

Waves in the Earth-ionosphere cavity

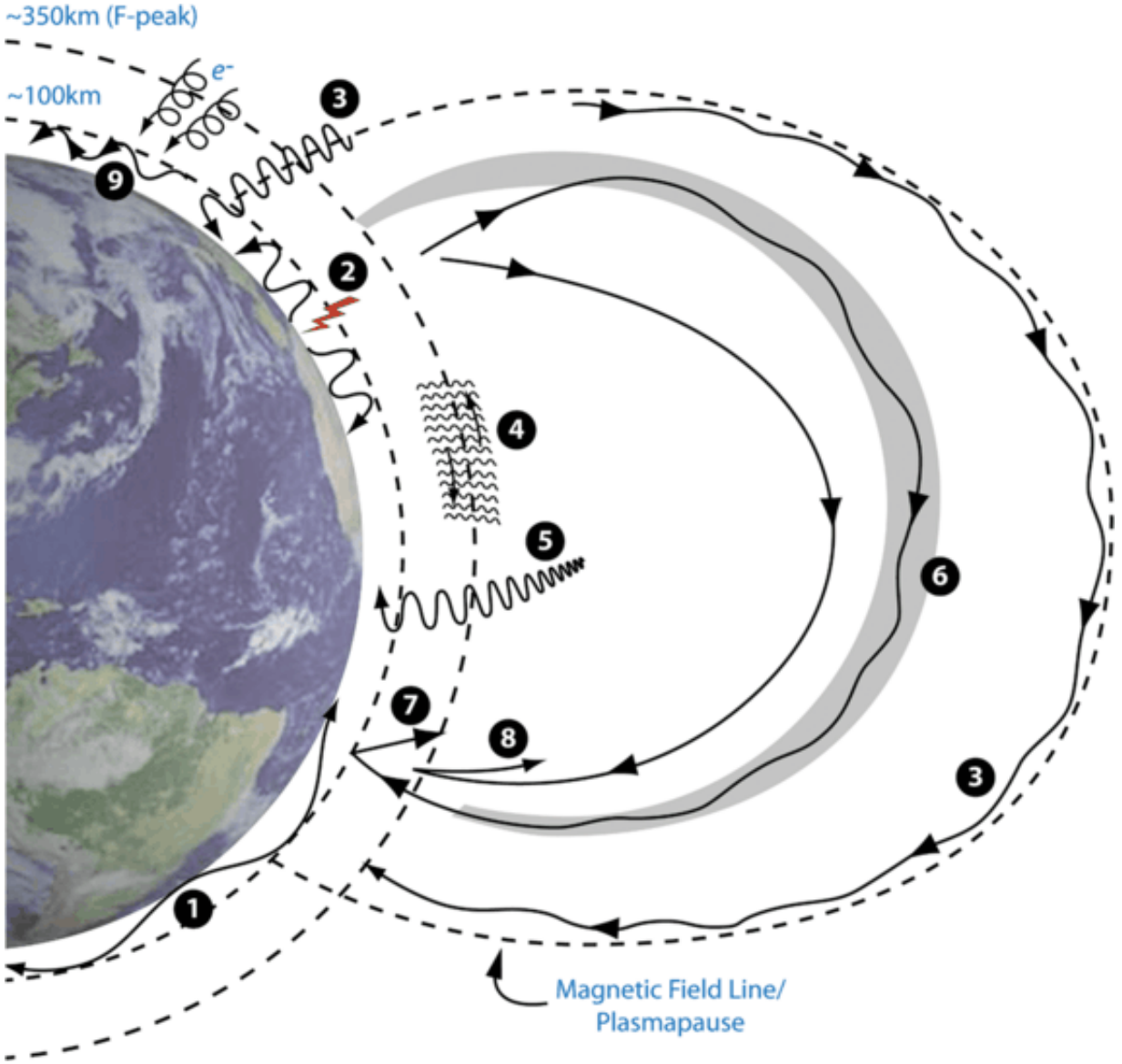

1. Schumann resonances.
2. Atmospherics.
3. Geomagnetic pulsations.
4. Alfvén waves (magnetosonic).
5. Alfvén waves (shear).
6. Whistler.
7. VLF propagation.
8. VLF reflection.
9. VLF subionospheric propagation.

Sketch of Low-frequency waves found in the troposphere-ionosphere. Extracted from *Simoes et al.* [2012].

F. Simoes, R. Pfaff, JJ. Berthelier, and J. Klenzing, A review of low frequency electromagnetic wave phenomena related to tropospheric-ionospheric coupling mechanisms, Space Sci Rev, 168:551-593, 2012.

Electricity in the atmosphere

There are around **2000 active storms** at every moment on the Earth. There are 4 equatorial-tropical areas where storms are more frequent: **Central Africa, South and Central America, Caribbean basin, and South-East Asia and Indonesia.**

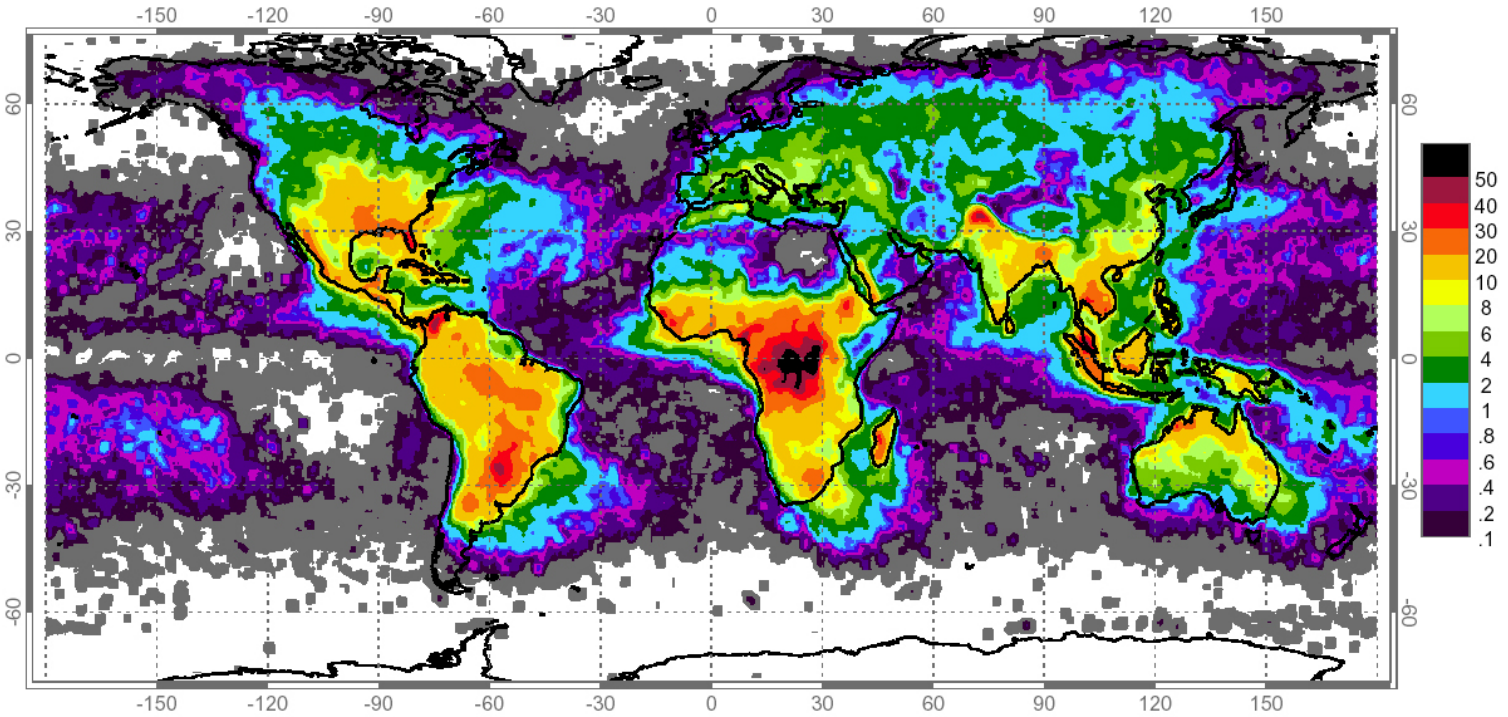

The annual distribution of total lightning activity [fl·km^{-2}·yr^{-1}]. Extracted from *Christian et al.* [2003].

H.J. Christian et al., Global frequency and distribution of lightning as observed from space by the Optical Transient Detector. *J. Geophys. Res.*, vol. 108(D1), pp. 4005, 2003.

The role of lightning

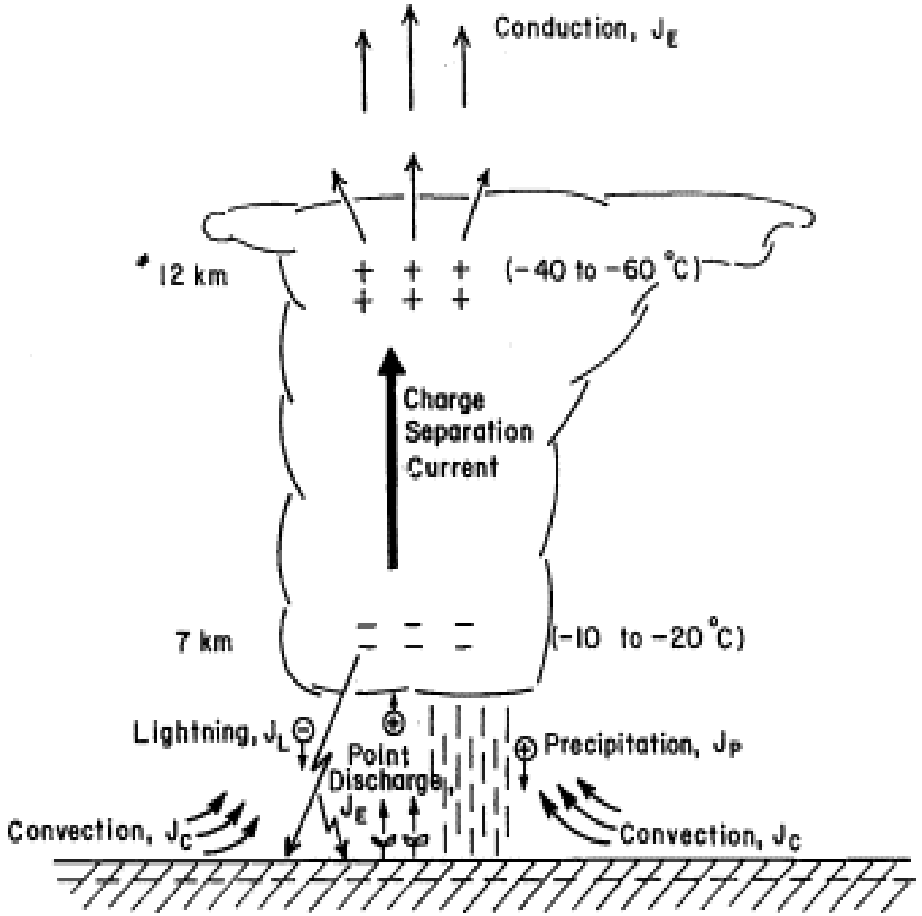

Generation of lightning. Extracted from *Siingh et al.* [*2005*].

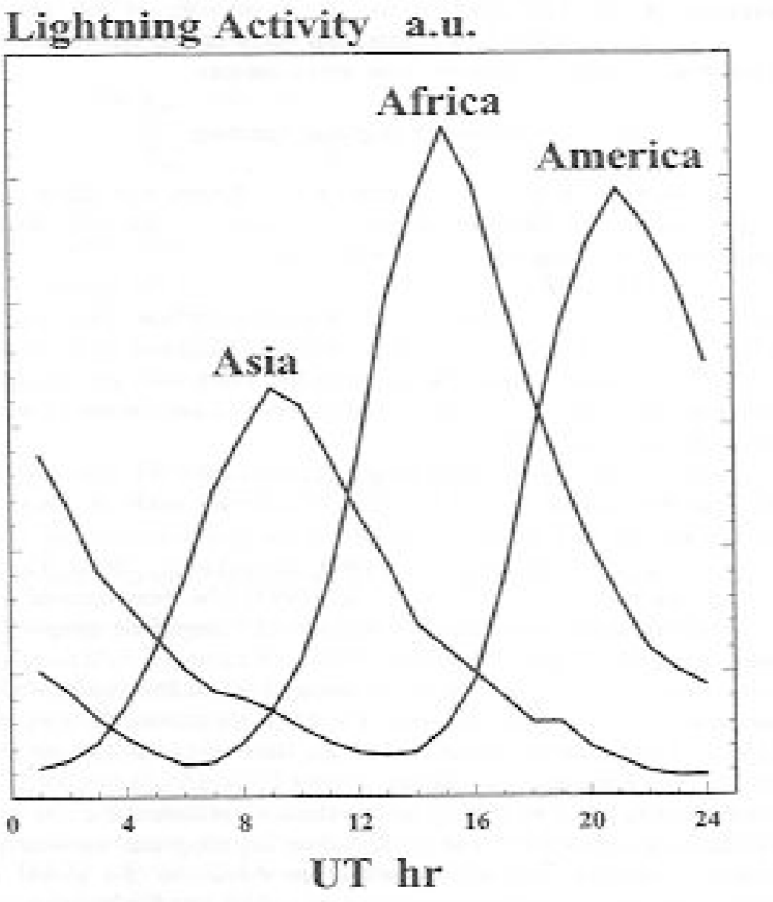

Influence of the three principal lightning basins. Extracted from *Nickolaenko and Hayakawa* [2002].

D. Siingh, RP. Singh, AK. Kamra, PN. Gupta, R. Singh, V. Gopalakrishnan, AK. Singh, Review of electromagnetic coupling between the Earth's atmosphere and the space environment, *J. Atm. Solar-Terr. Phys.*, 67, 637-658, 2005.

Seismo-electromagnetism

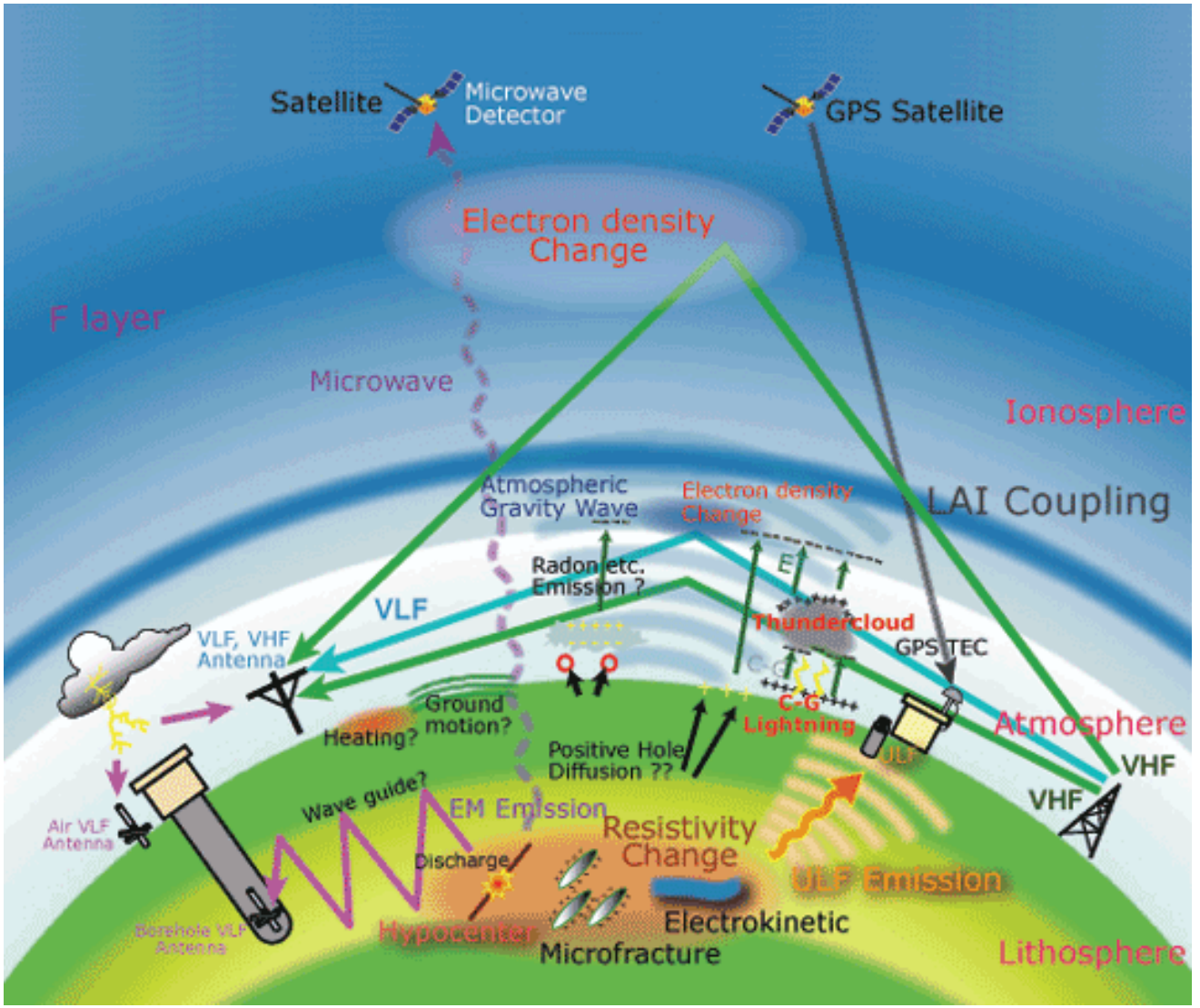

Extracted from *www.isfep.com*
ISFEP stands for International Society For Earthquake Precursors.

Typical Schumann resonance spectrum

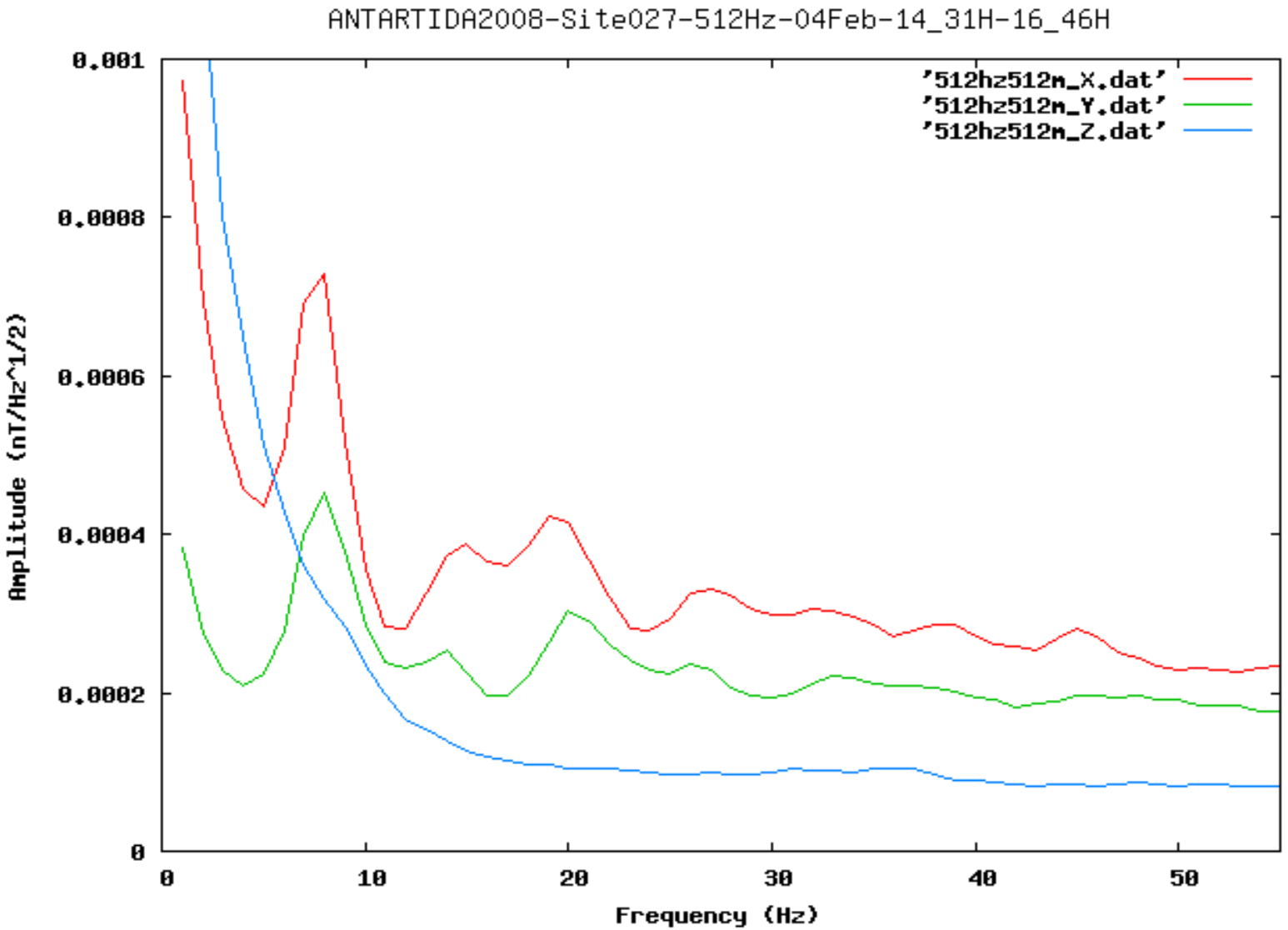

SR spectrum recorded the 4th February 2008 in Antarctica. Up to 8 resonances can be observed.

Spherical shell cavity of perfect conductors, no losses

Amplitude of Schumann resonance modes for a source located at θ=0 (North Pole).

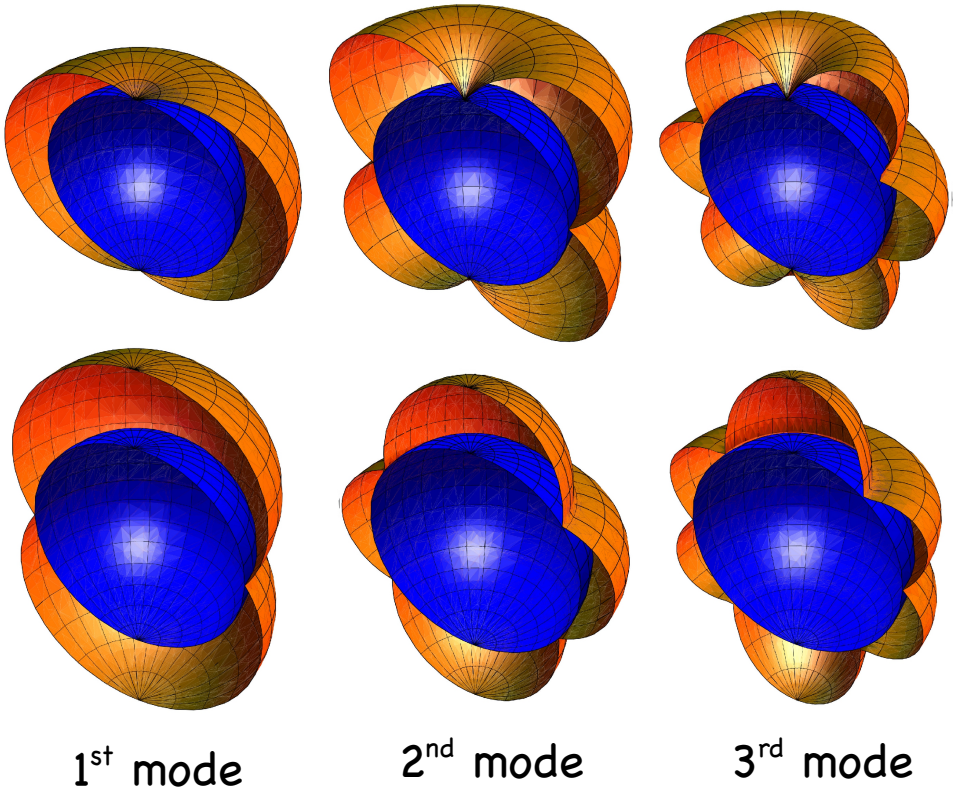

Mode frequencies TM^r	
n=1	$f_r = 10{,}51 Hz$
n=2	$f_r = 18{,}21 Hz$
n=3	$f_r = 25{,}75 Hz$
n=4	$f_r = 33{,}24 Hz$
n=5	$f_r = 40{,}71 Hz$
n=6	$f_r = 48{,}17 Hz$
n=7	$f_r = 55{,}62 Hz$
n=8	$f_r = 63{,}07 Hz$
n=9	$f_r = 70{,}51 Hz$
n=10	$f_r = 77{,}95 Hz$

$$H_\phi = \frac{1}{\mu r}\left(A\hat{J}_n(\beta r) + B\hat{Y}_n(\beta r)\right)\frac{\partial}{\partial\theta}\left(P_n(cos\theta)\right)$$

$$E_r = \frac{1}{j\omega\mu\varepsilon}\left[\left(\frac{\partial^2}{\partial\theta^2} + \beta^2 P_n(cos\theta)\right)\left(A\hat{J}_n(\beta r) + B\hat{Y}_n(\beta r)\right)\right]$$

The Transmission-Line Modelling method (TLM)

The **TLM** is a **numerical method**, devised in **time domain**, which approaches to the problem by defining a **transmission line circuit** which behaves in a similar manner, i.e. is governed by the **same differential equations**. The time and space are discretized, and a cell unit or TLM node is assigned to each differential of volume.

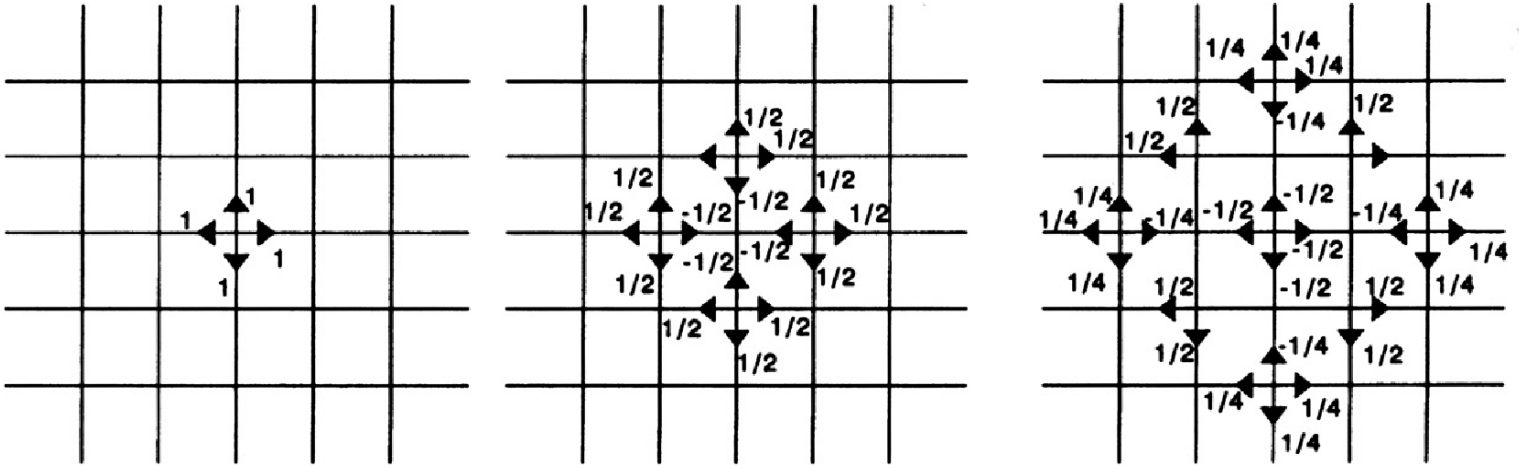

Evolution of the pulses traveling in a TLM mesh.

At each time step, every node transforms its incident pulsed V_i into reflected pulses V_r by means of the **scattering matrix**, *S,* which defines the node.

$$V_n^r = SV_n^i$$

C. Christopoulos, *The Transmission-line modeling method: TLM,* The institute of Electrical and Electronic engineers, Piscataway, NJ, 1995.

Numerical model (TLM) of the Earth-ionosphere cavity

- The cavity is modeled as **two perfect conducting spheres,** lithosphere (r_1=6370 km) and lower ionosphere (r_2=6470 km). The **height of the atmosphere is 100 km**.
- The **knee model** is employed for the **varying conductivity** of the atmosphere.
- The space between the conducting spheres is modeled by cubes of size **10 km**, leading to ~$5 \cdot 10^7$ cubes.
- $2.4 \cdot 10^5$ time iterations are computed (i.e. **4 seconds**), leading to **0.25 Hz** of frequency resolution. **36 hours** of **computation** required on a 32 cpu computer.

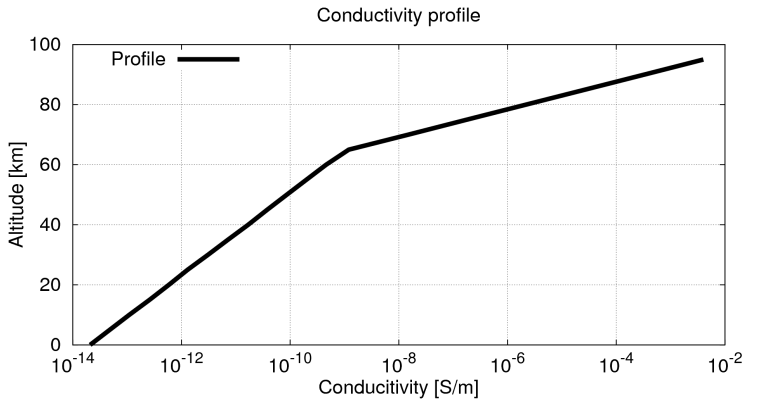

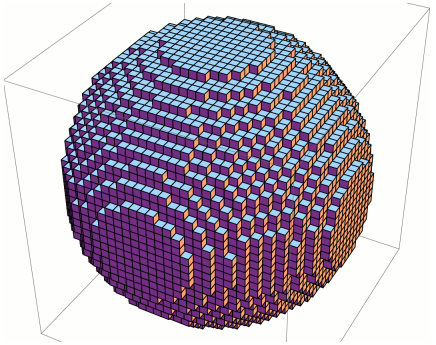

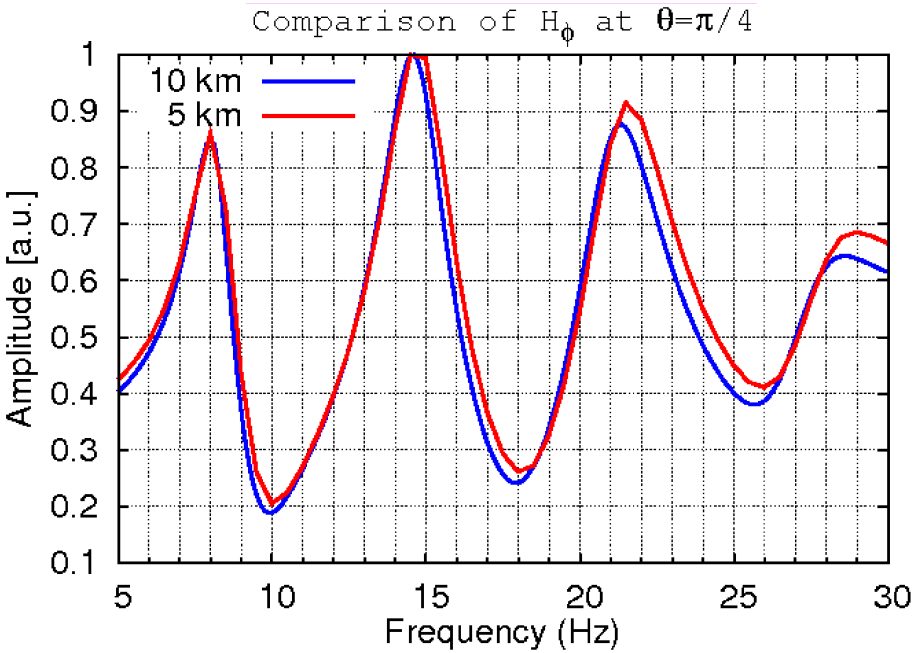

S. Toledo-Redondo, A. Salinas, J.A. Morente-Molinera, A. Méndez, J. Fornieles, J. Portí, and J.A. Morente, Parallel 3D-TLM algorithm for simulation of the Earth-ionosphere cavity, *J. Comp. Phys.*, 236, 367–379, 2013.

Lossless Earth-ionosphere cavity

Results of the model for a **cavity without a conductivity profile**, with nodes of size 5 and 10 km. The results are in good agreement with the theoretical results.

[Hz]	1st SR	2nd SR	3rd SR	4th SR	5th SR	6th SR
10 km	10.24	17.74	24.98	32.35	39.63	46.93
5 km	10.47	17.99	25.48	32.96	39.98	47.47
Analytical	10.51	18.20	25.75	33.24	40.71	48.17

The **error** of the SR frequencies is **less** than **3%** for 10 km cell size and less than **1.5%** for 5 km cell size.
The required **computation time** was roughly **21 hours** and **7 days** respectively, on a 32 cores computer.

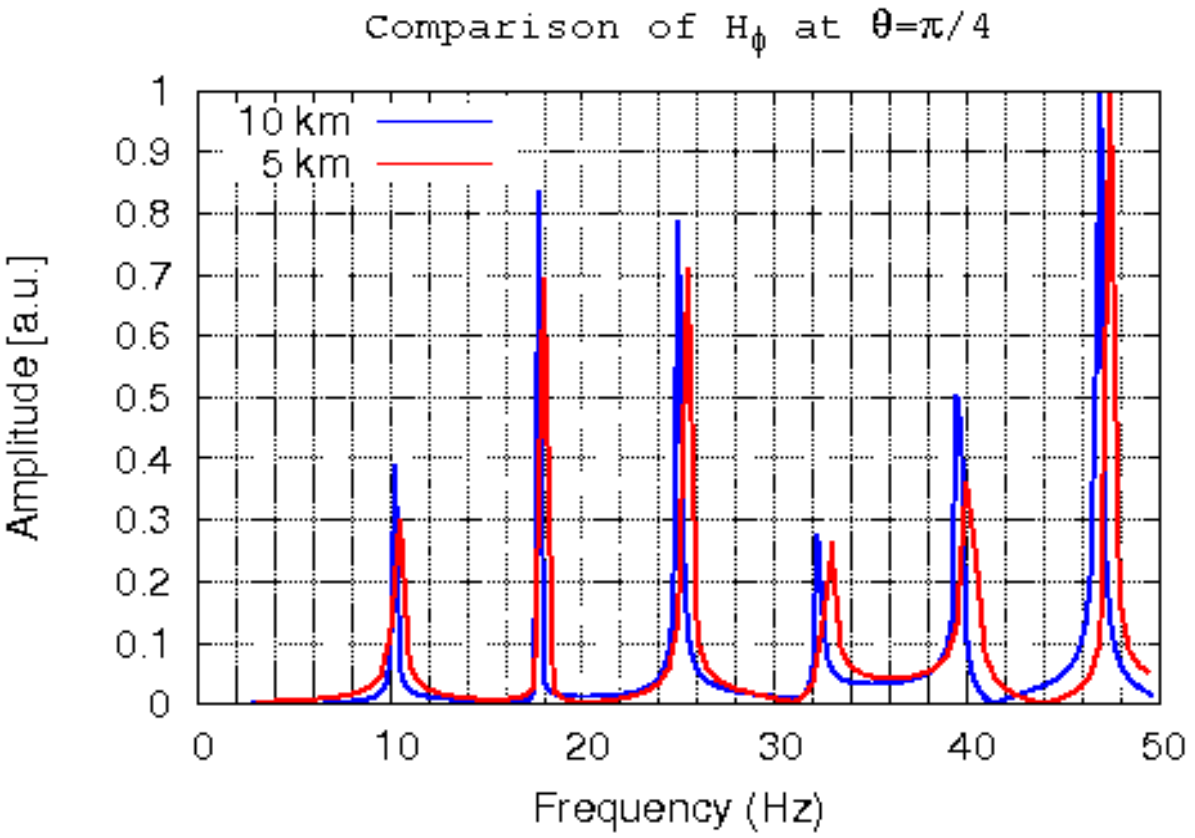

Earth-ionosphere cavity model, modal amplitude variations

The amplitude dependence with distance to the source obtained numerically by means of TLM is in perfect agreement with analytical models.

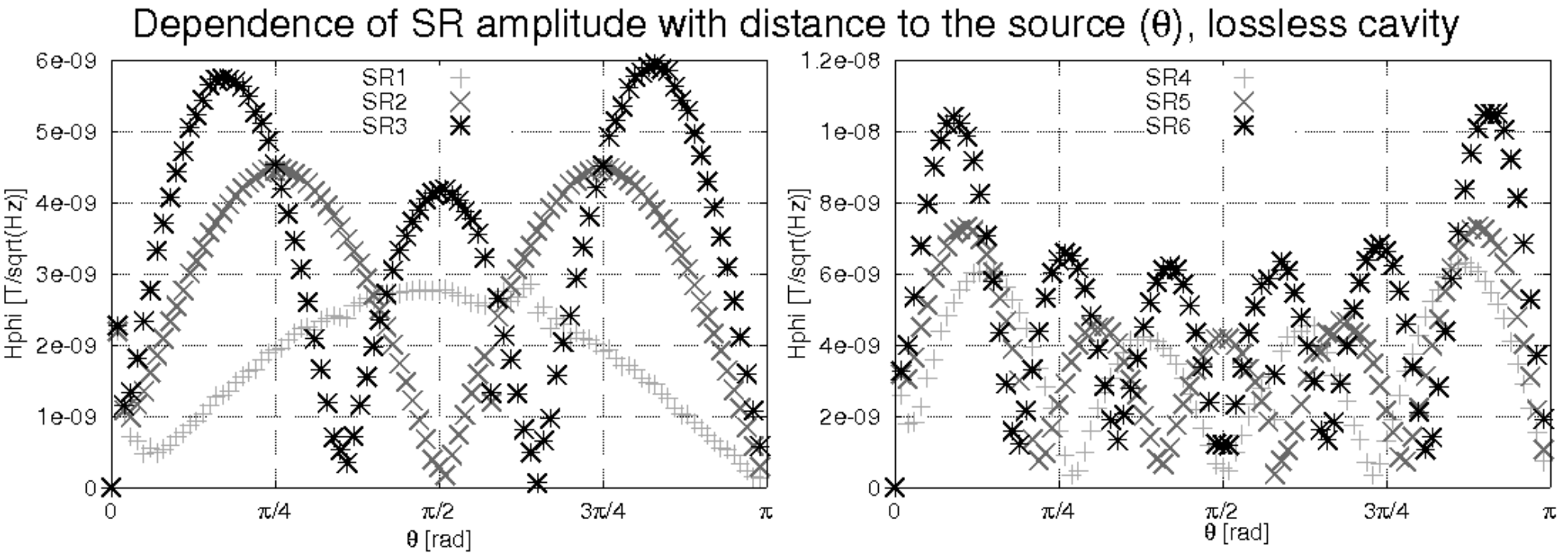

Lossy Earth-ionosphere cavity

Results of the model for a **cavity with a conductivity profile**, with nodes of size 5 and 10 km. The results are in good agreement with the theoretical results.
For the lossy cavity, **the SR frequency depends on the distance to the source.** This is in agreement with the recent measurements made by *Satori et al*. [2012].

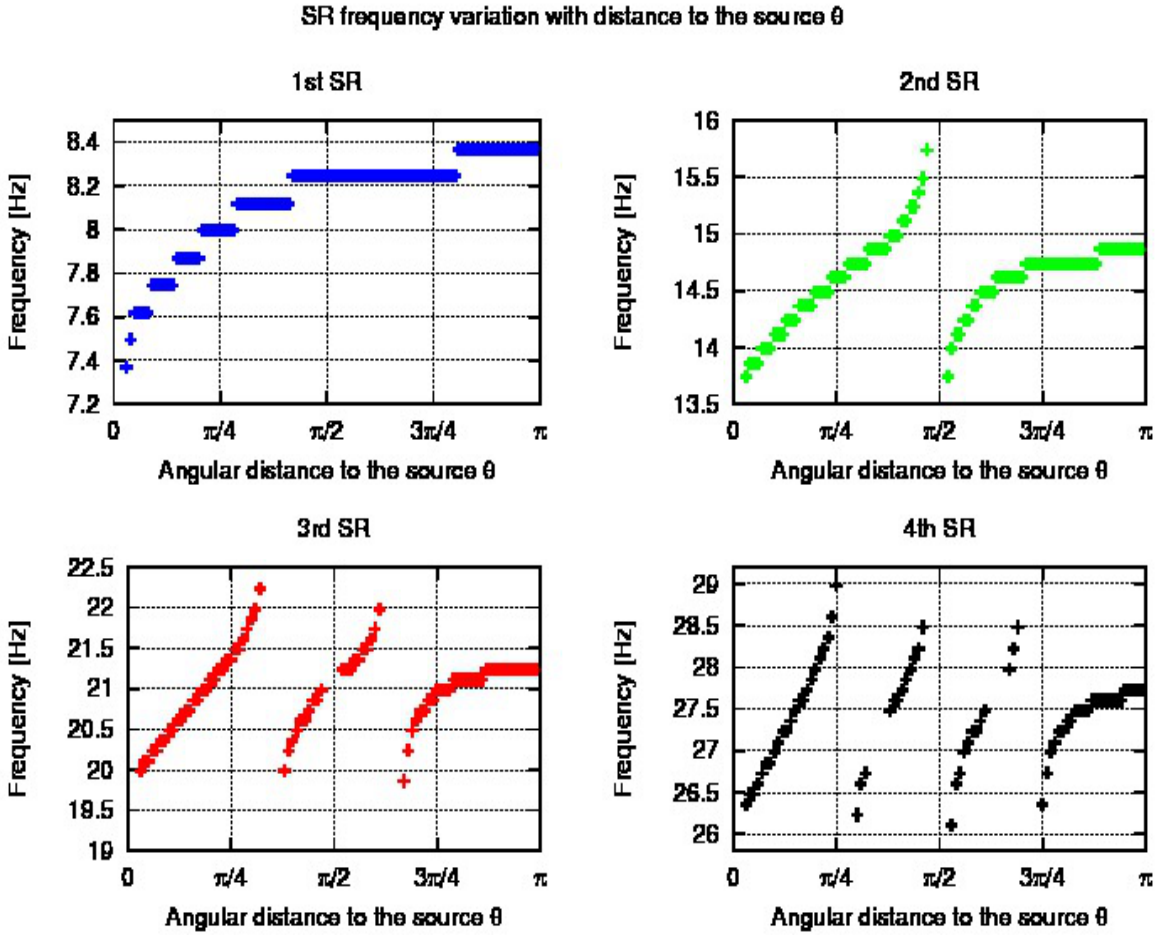

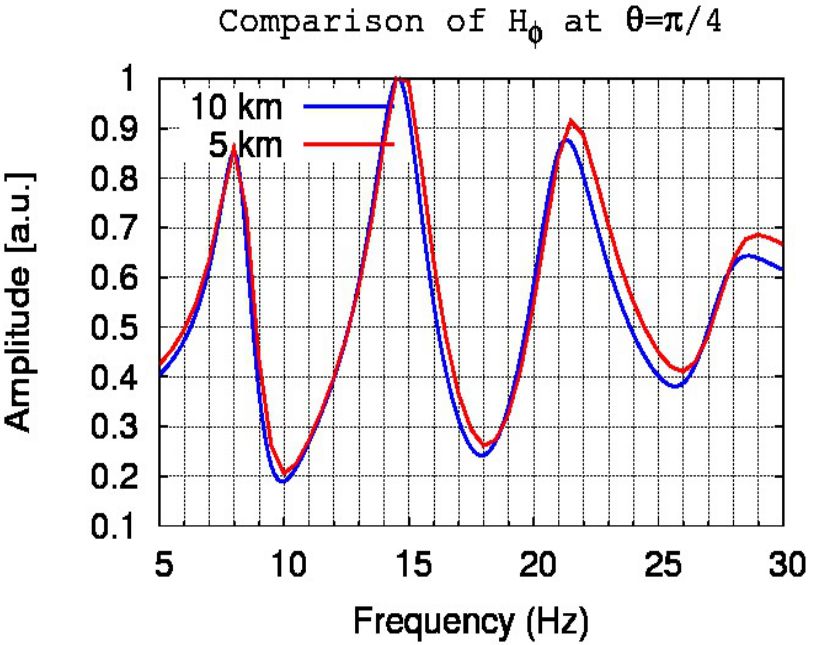

For the lossy cavity, the central SR frequencies have lower value and the **Q-factors** are also lower.

G. Satori, V. Mushtak, M. Neska, T. Nagy, and V. Barta, Global lightning dynamics deduced from Schumann resonance frequency variations at two sites ~ 550 km apart, *European Geosciences Union General Assembly*, Vienna, 22-27 April 2012.

Earth-ionosphere cavity model, frequency variations

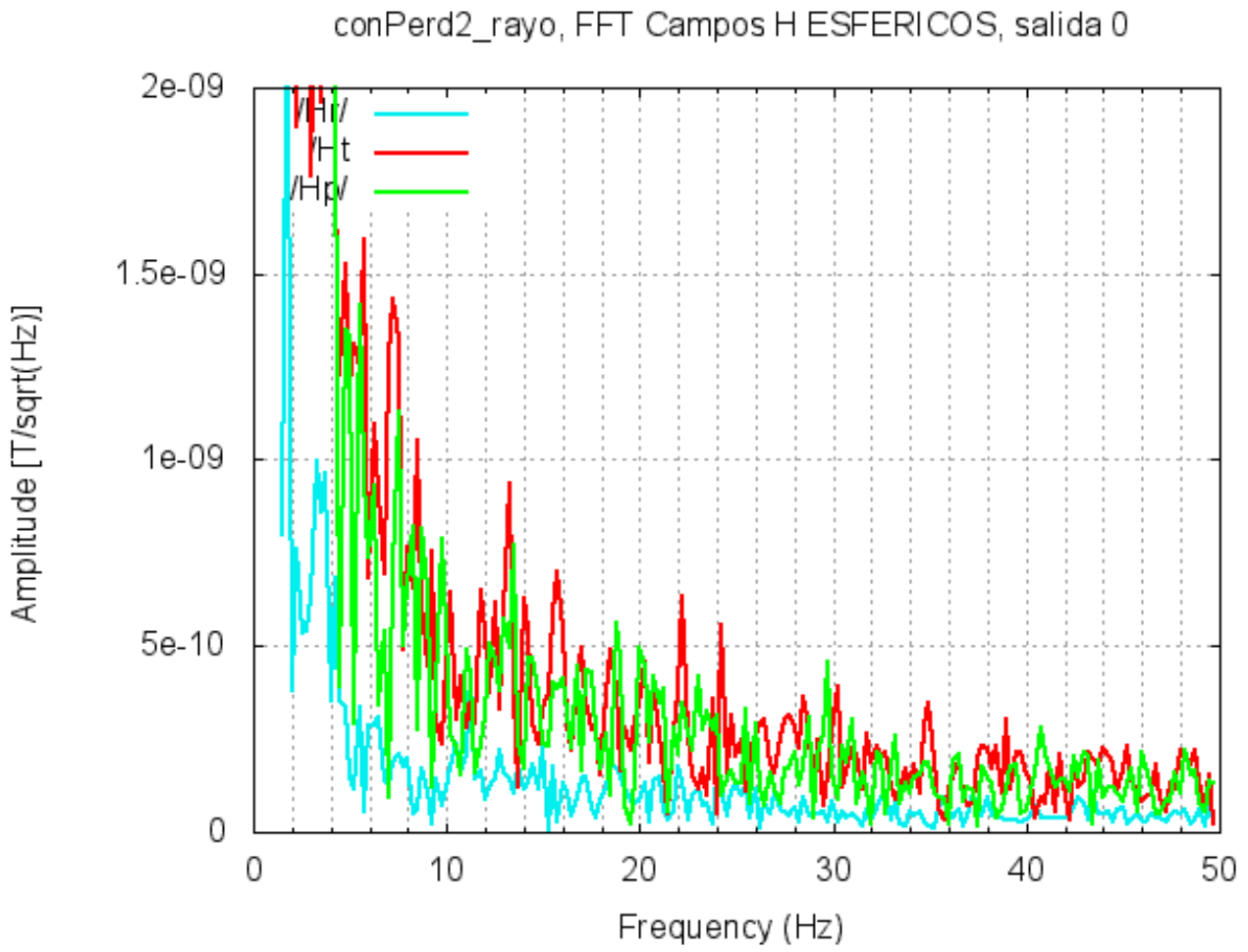

Effect of hypothetical Eq. Precursors on the SR

- The **source** (single +CG lightning) is placed at the **North Pole** (NP), or θ = 0.
- Earthquake precursor is fixed: location (**θ**), magnitude (**M**), and conductivity variation (**h**).
- **Observation points** are placed **along the θ coordinate**.
- **Poynting vector** is employed as a **measurement** parameter of Schumann resonances.

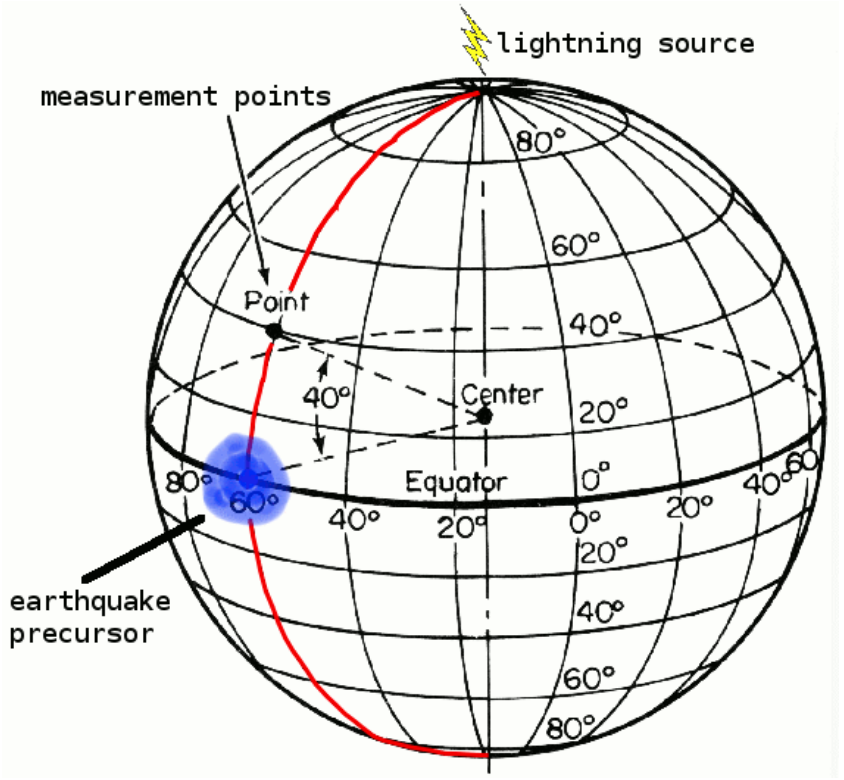

$$\vec{P} = \frac{1}{2} Re\left[\vec{E} \times \vec{H}^{*}\right]$$

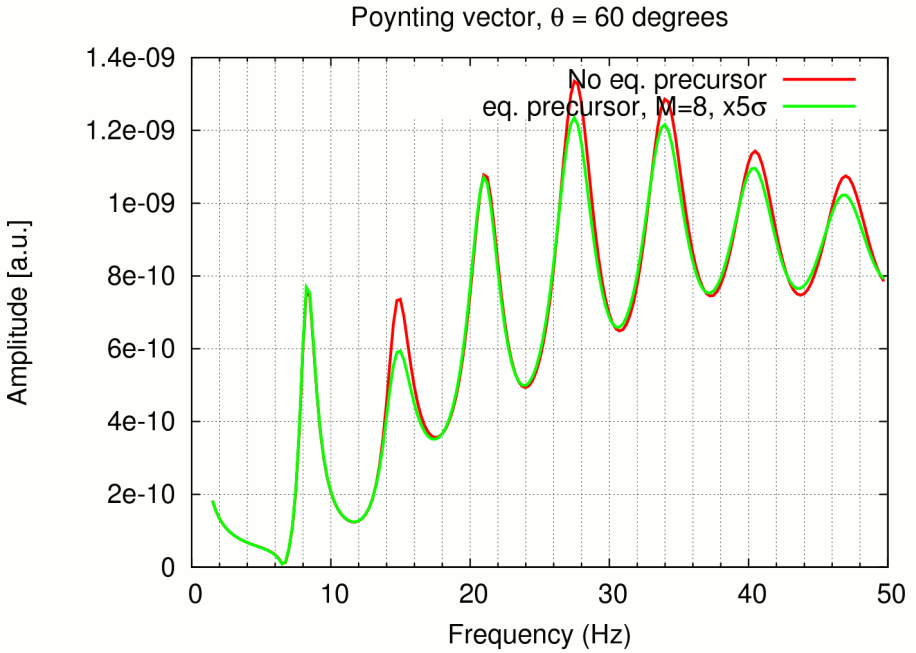

Poynting vector variation for hypothetical M=8 Eq. precursor

$$10\log_{10}\left[\frac{P_{Eq}(f)-P_{Reg}(f)}{\bar{P}_{\theta}}\right]$$

h=5 km, M=8 (r=2500 km)

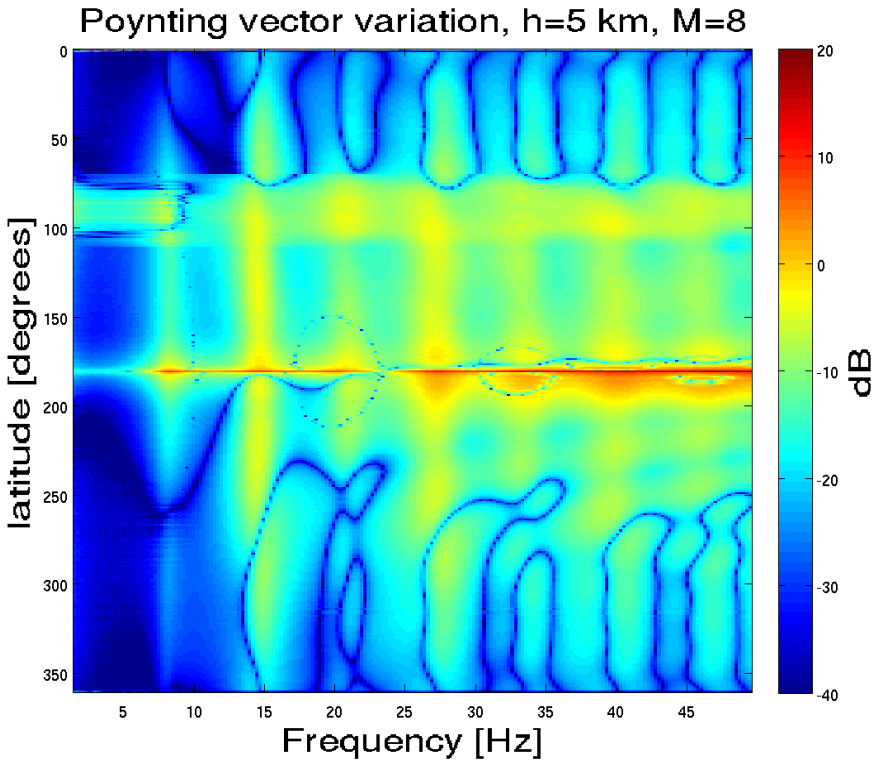

h=10 km, M=8 (r=2500 km)

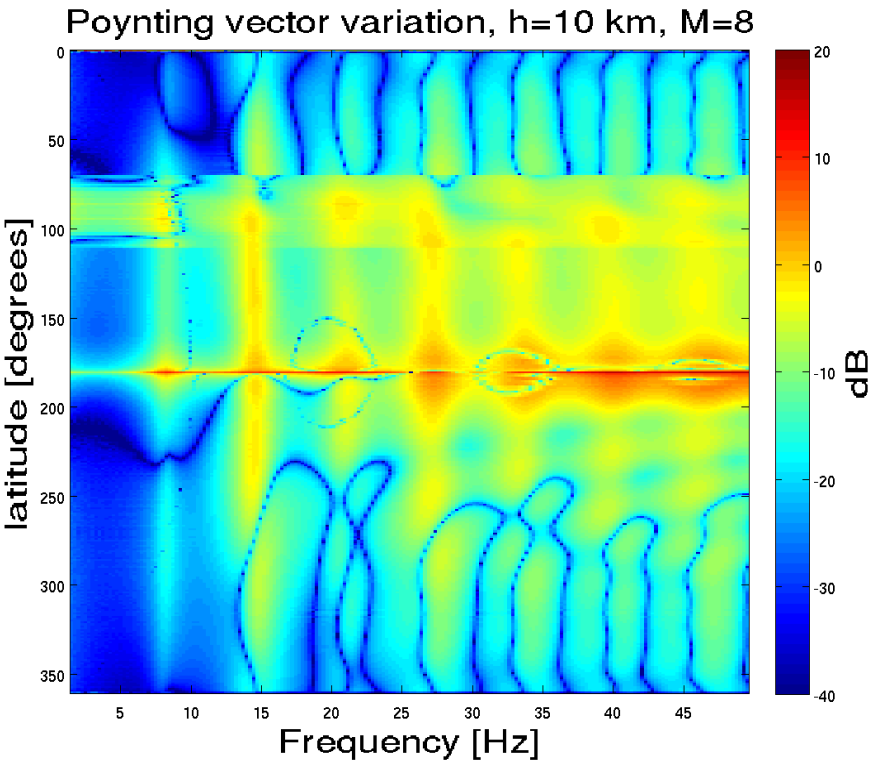

Poynting vector variation for hypothetical M=7 Eq. precursor

$$10\log_{10}\left[\frac{P_{Eq}(f)-P_{Reg}(f)}{\bar{P}_{\theta}}\right]$$

h=5 km, M=7 (r=1000 km)

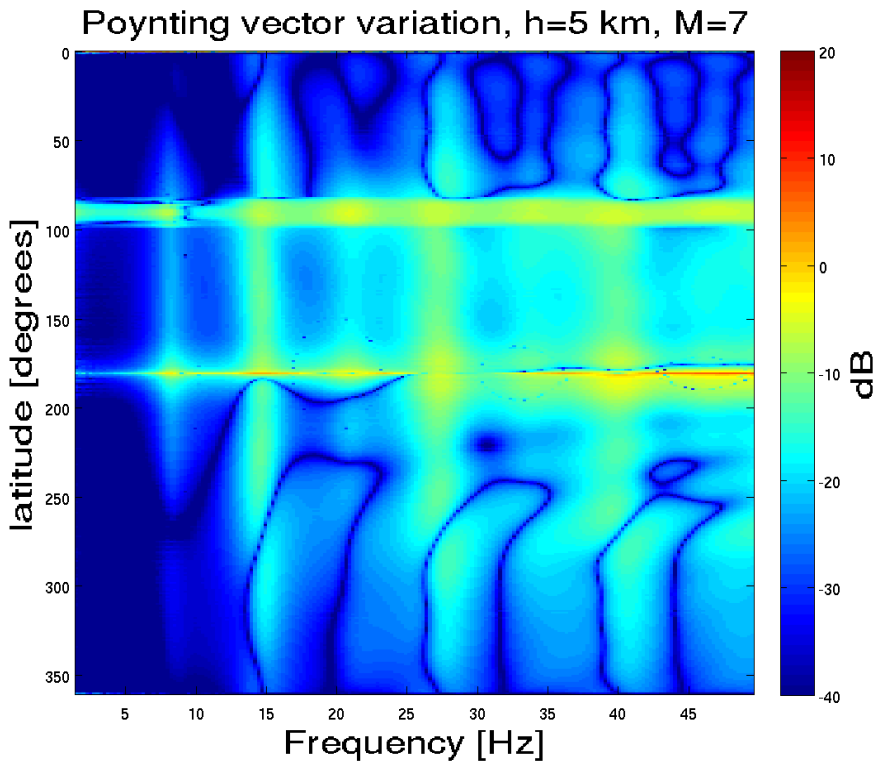

h=10 km, M=7 (r=1000 km)

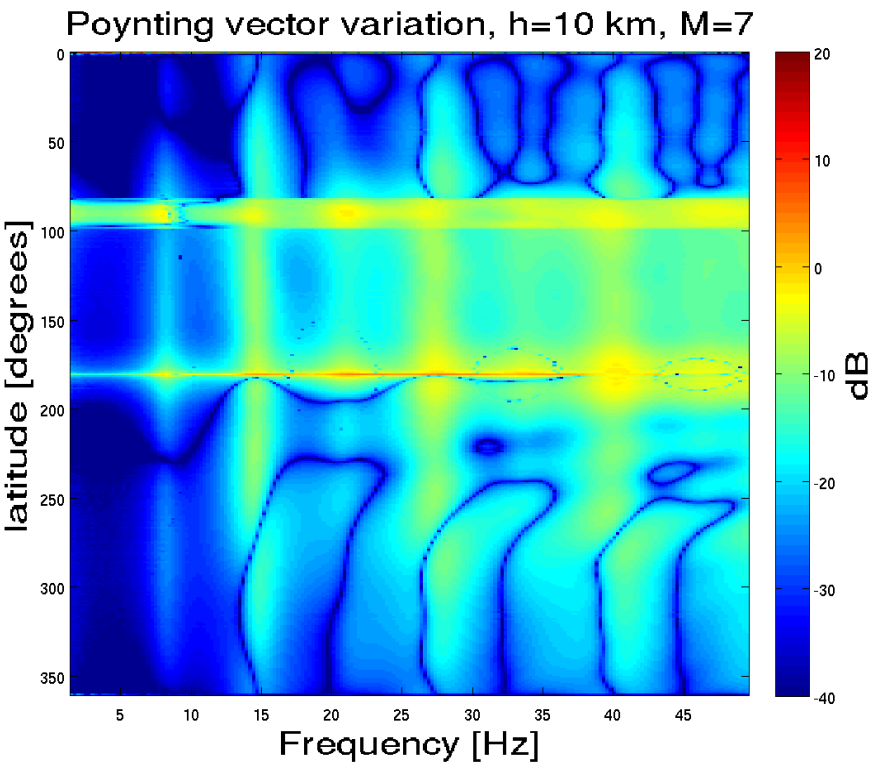

Poynting vector variation for hypothetical M=6 Eq. precursor

$$10\log_{10}\left[\frac{P_{Eq}(f)-P_{Reg}(f)}{\bar{P}_{\theta}}\right]$$

h=5 km, M=6 (r=380 km)

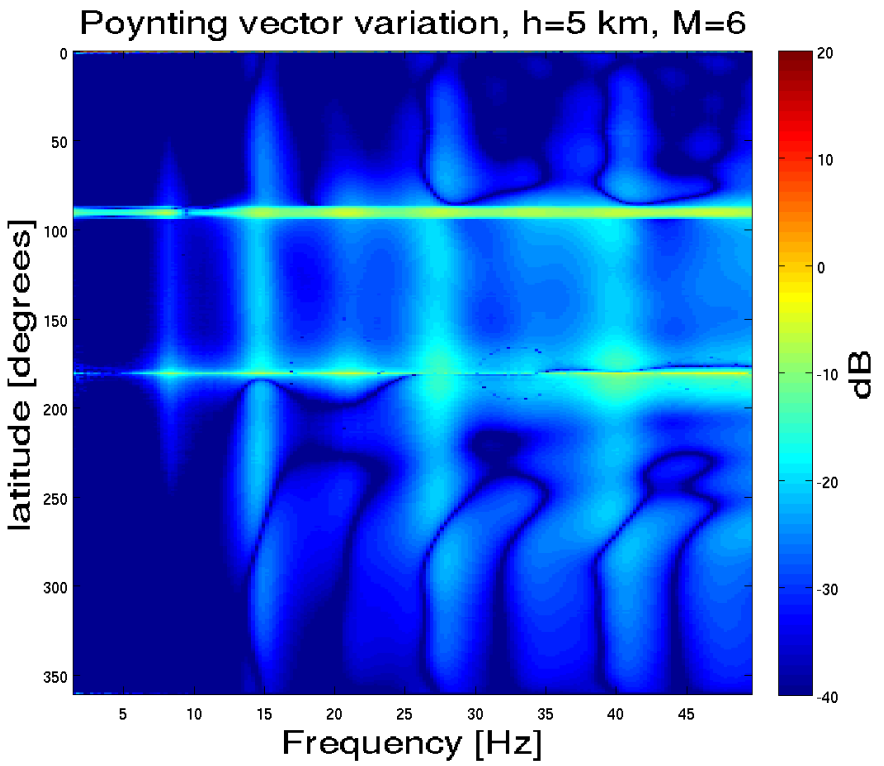

h=10 km, M=6 (r=380 km)

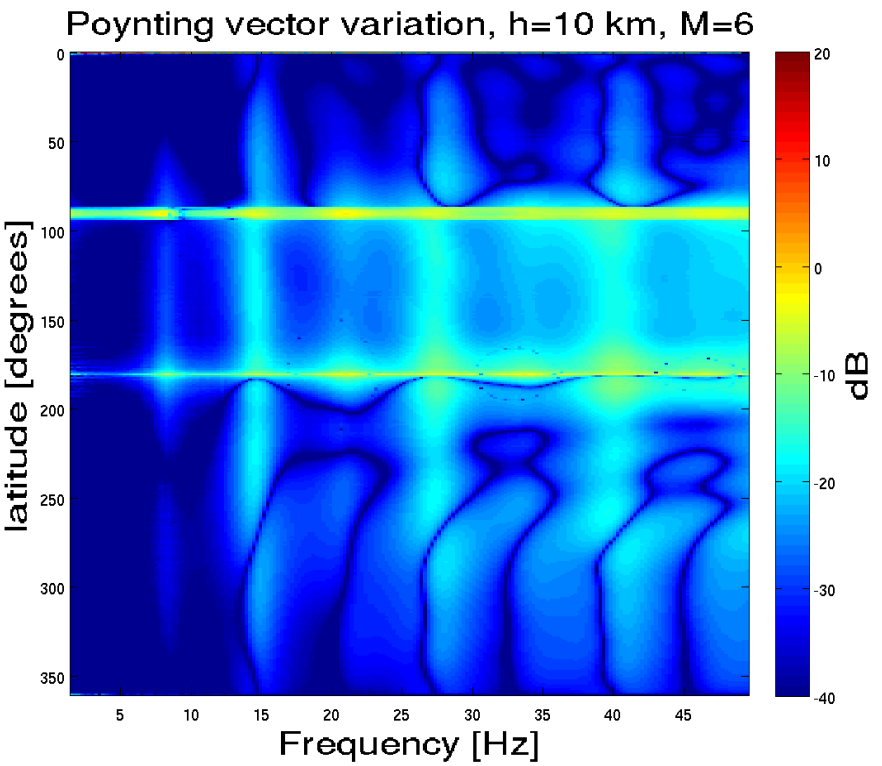

Case of study: Taiwan Earthquake 26-12-2006

- **Earthquake**: M=7.3 (r=1377 km), epicenter in **Taiwan** (22º N, 120.48º E).
- **Observation** point: **Moshiri** SR station (44.29º N, 142.21º E).
- The **source** point is supposed to be in the **American Basin** (0º N, 50 ºW).

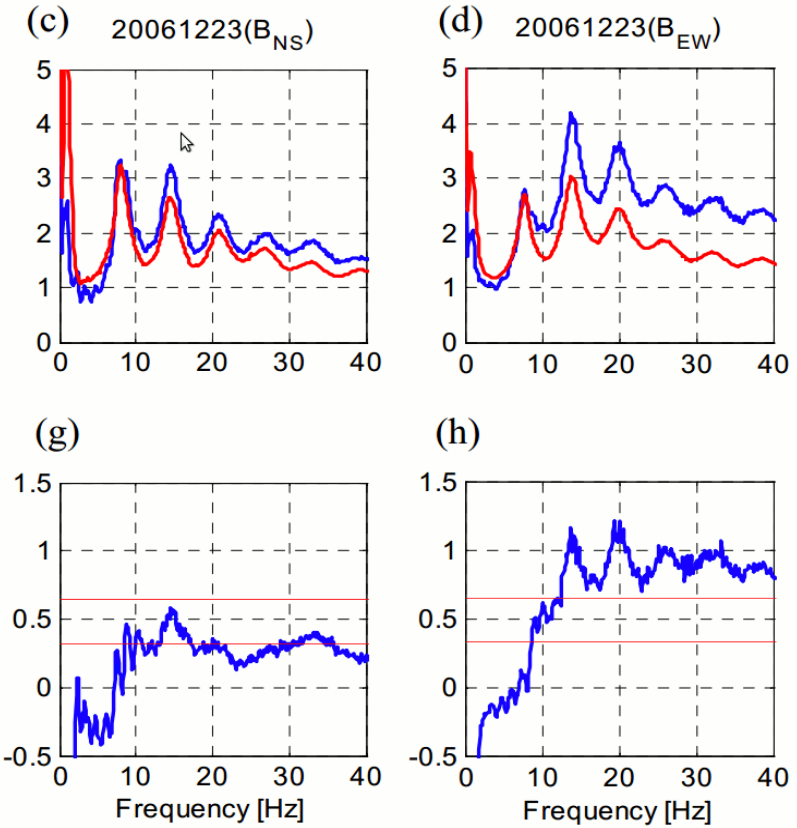

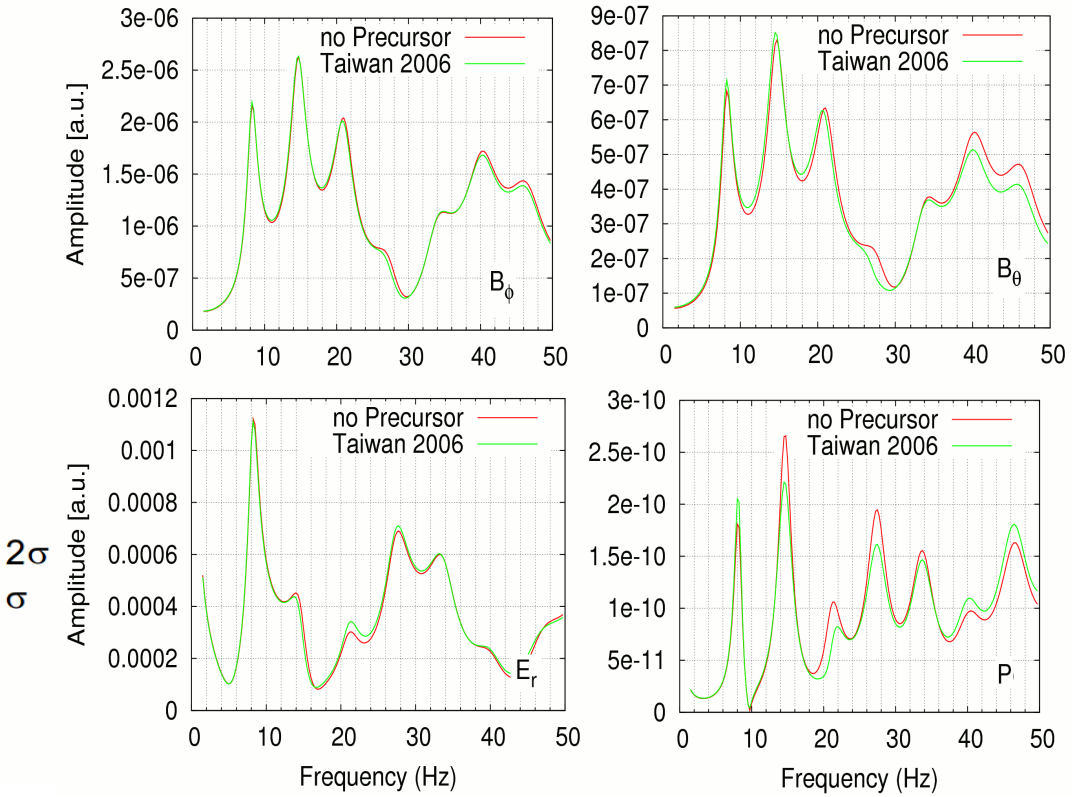

Extracted from *Hayakawa et al.* [2008].

Results from TLM model.

M. Hayakawa et al., Anomalous ELF phenomena in the Schumann resonance band as observed at Moshiri (Japan) in possible association with an earthquake in Taiwan, *Nat. Hazards Earth Syst. Sci., 8*, 1309-1316, 2008.

Case of study (II): Chi-chi earthquake 21-09-1999

- **Earthquake**: M=7.6 (r=1850 km), epicenter in **Chi-chi**, Taiwan (23.77º N, 120.98º E).
- **Observation** point: **Nakatsugawa** SR station (35.4º N, 137.5º E).
- The **source** point is supposed to be in the **American Basin** (0º N, 50 ºW).

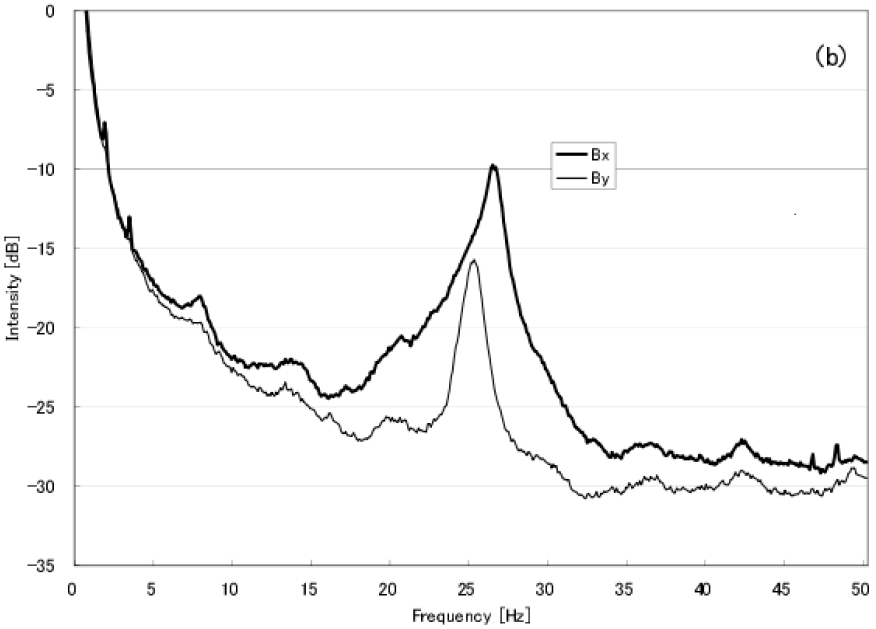

Extracted from *Hayakawa et al.* [2005.]

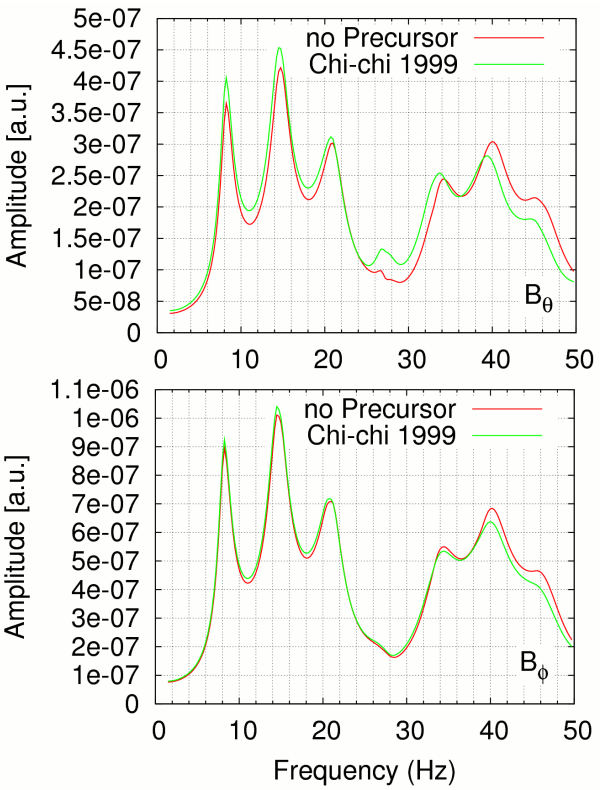

Results from TLM model

M. Hayakawa et al., Anomalous ELF phenomena in the Schumann resonance band as observed in Japan, possibly associated with the Chi-chi earthquake in Taiwan, *Annales Geophysicae, 23*, 1335-1346, 2005.

Day-night asymmetry

The cavity with different conductivity profiles for day and night has been modeled for an equinox day. The source (single lightning) is located at the equator, at 4 different local times: 00h, 06h, 12h, 18h.

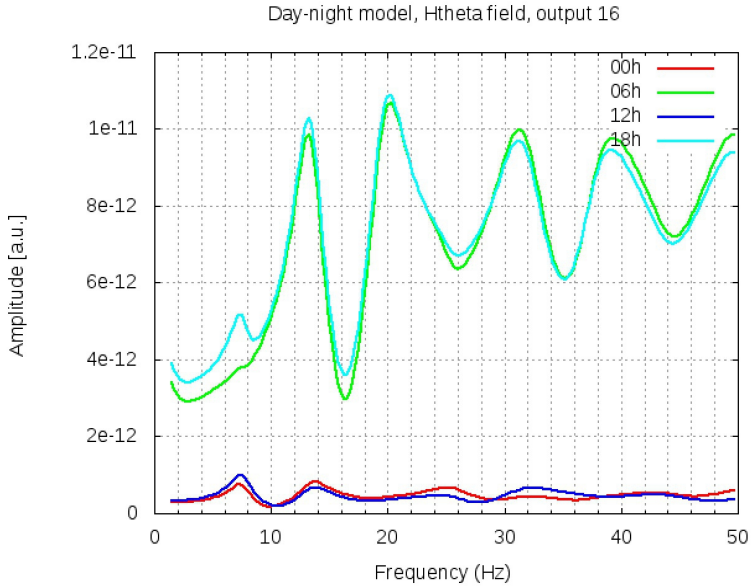

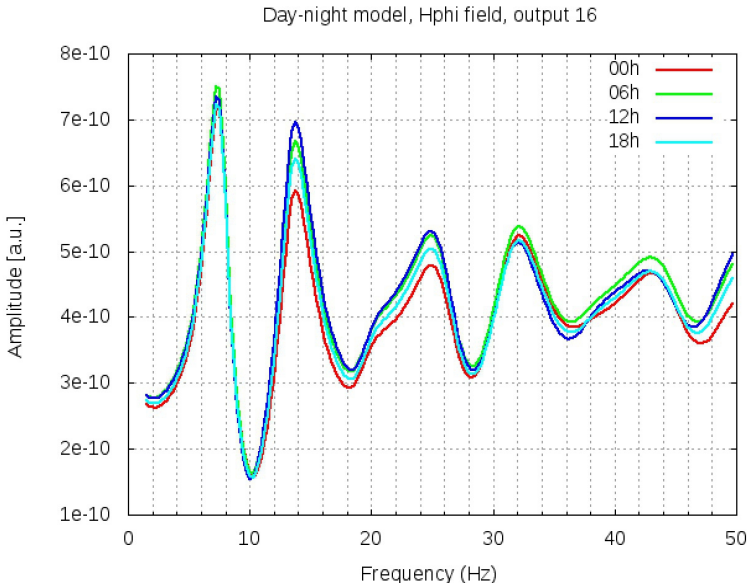

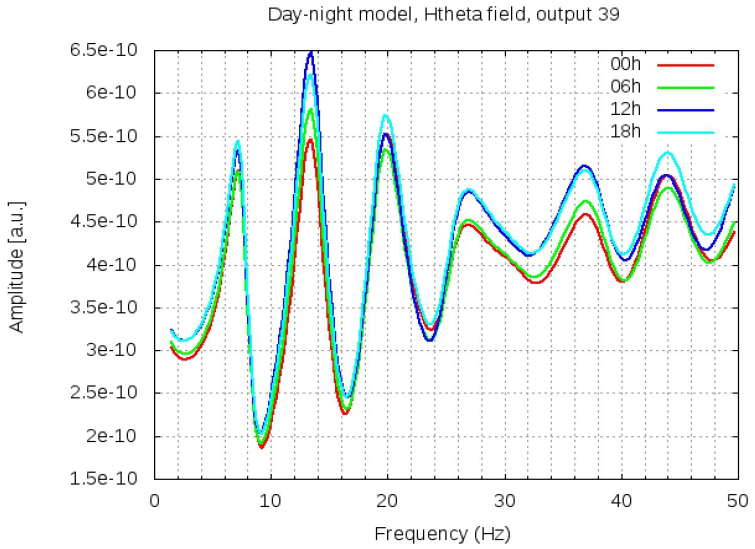

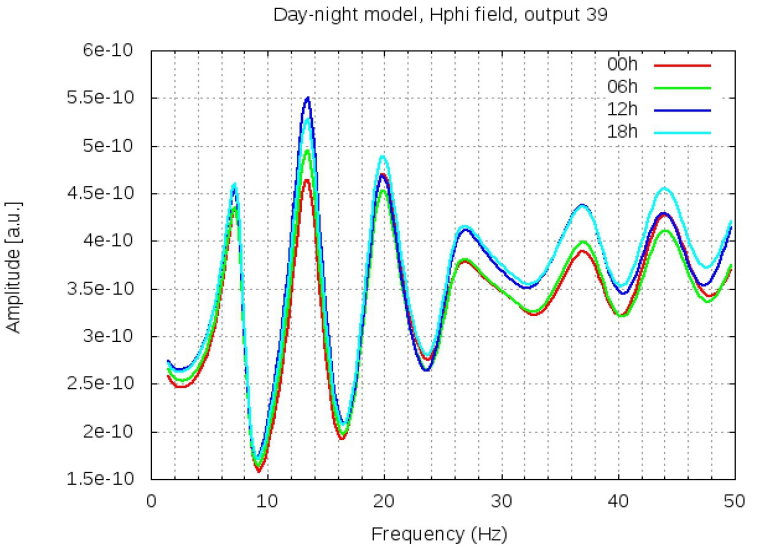

Picture of the **terminator** over the Earth.

Spectral analysis of Schumann resonance records

Bartlett's Method

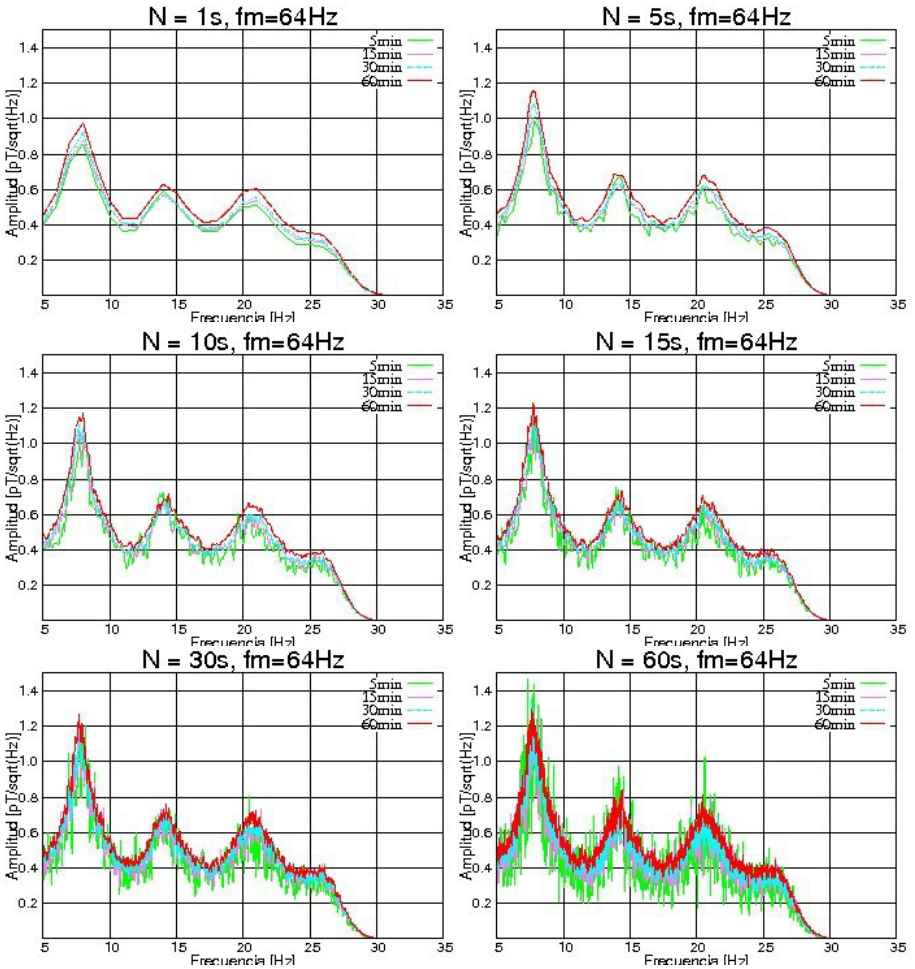

Lorentzian Fit

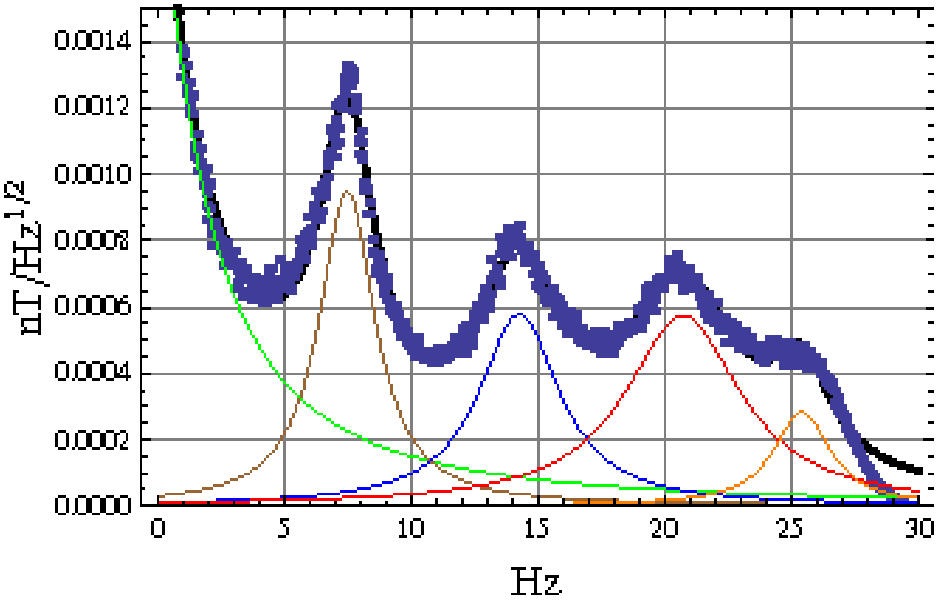

$$F_{lor} = \sum_{n=0}^{N} \frac{B_n}{\left(\frac{f - f_{max,n}}{\Delta f_n} \right)^2 + 1}$$

Bartlett's spectral estimation reduces noise at the cost of reducing the frequency resolution of the Fourier Transform.

The Lorentzian fit of each resonance permits to quantify them in terms of amplitude, central frequency, and quality factor.

The Magnetotelluric method

Deployment of sensors in magnetotelluric campaigns. **Three magnetic field components plus two electric field components are recorded.**

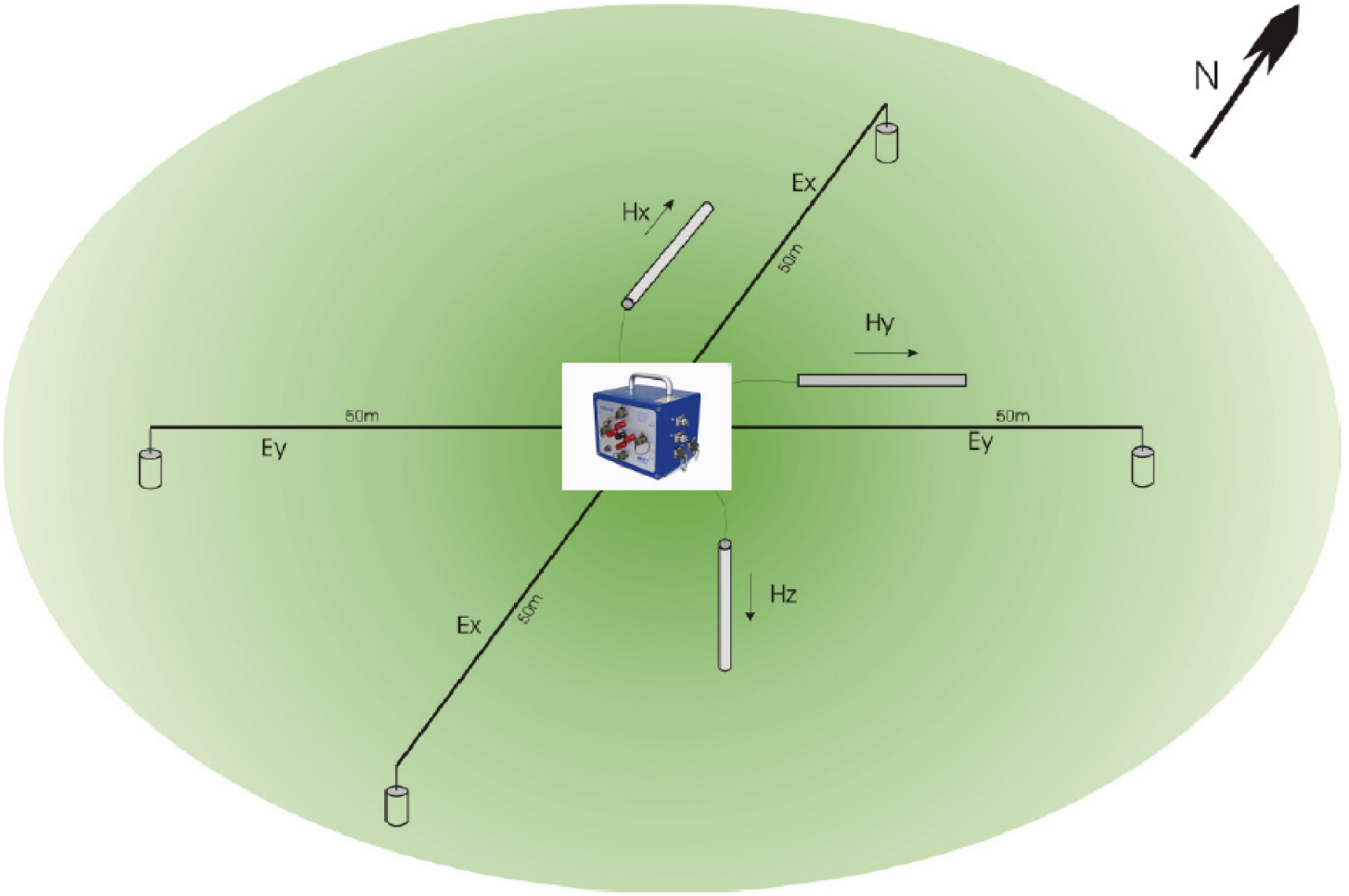

L. Cagniard, Basic theory of the magnetotelluric method of geophysical prospecting, *Geophysics*, vol. 18(3), pp. 605-635, 1953.

MT surveys in Spain, Morocco and Antarctica

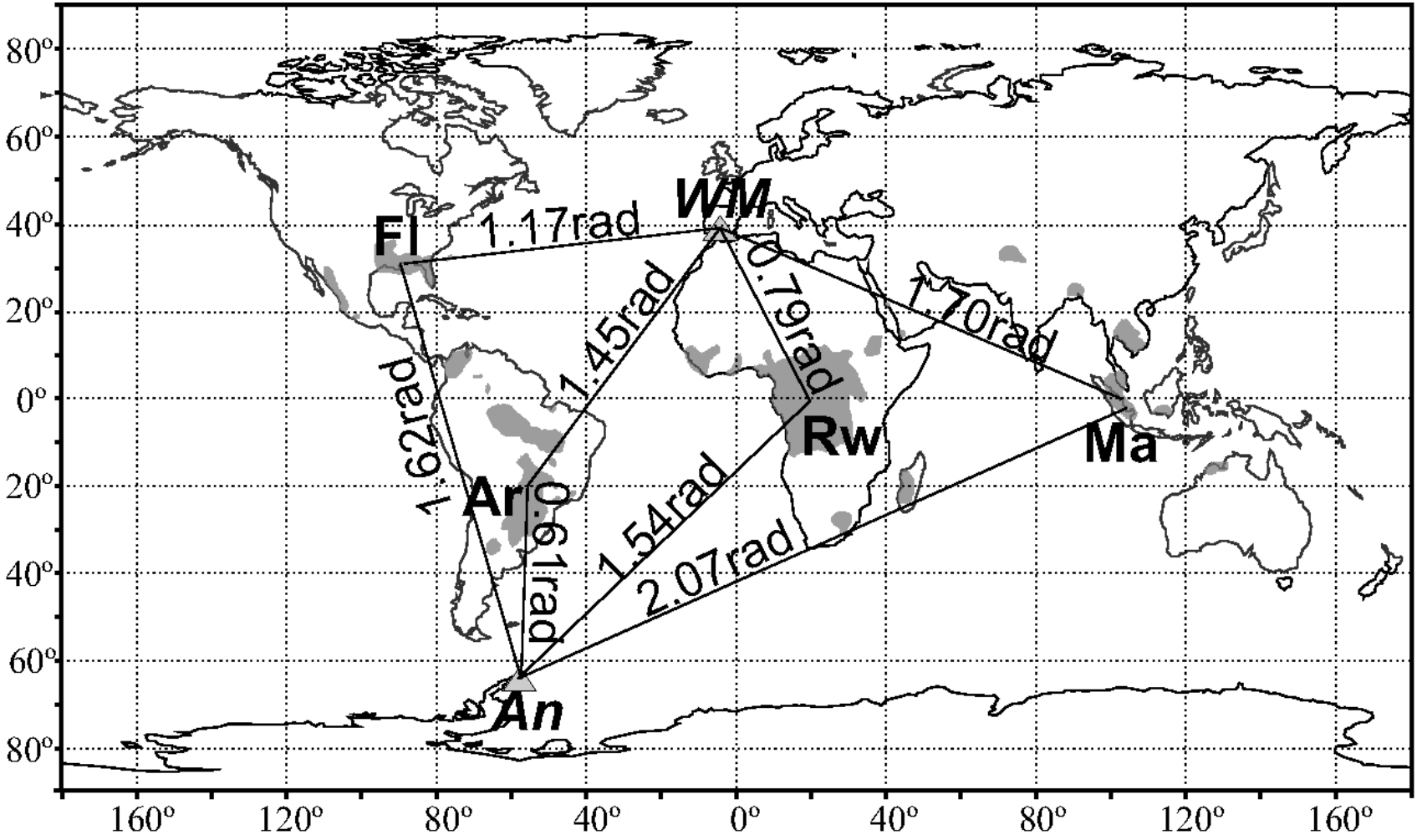

Location of the MT campaigns of this study (**Western Mediterranean** and **Antarctica**), and distance to the main storm centers (Malaysia, Rwanda, Florida, and Argentina).

S. Toledo-Redondo, A. Salinas, J. Portí, J.A. Morente, J. Fornieles, A. Méndez, J. Galindo-Zaldívar, A. Pedrera, A. Ruiz-Constán, and F. Anahnah, Study of Schumann resonances based on magnetotelluric records from the western Mediterranean and Antarctica. *J. Geophys. Res.*, vol. 115, pp. D22114, 2010.

SR spectrograms

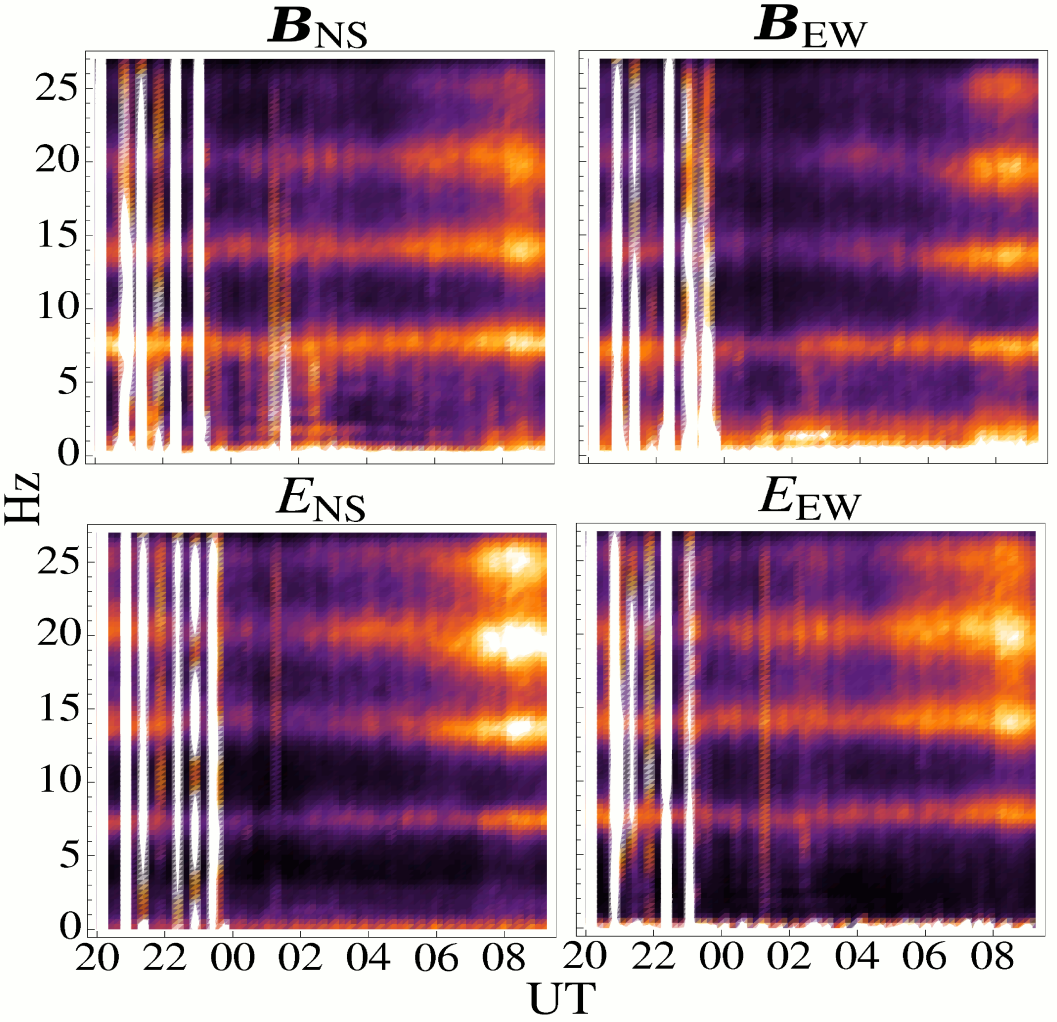

Spectrogram 14 hours long,Morocco survey, 5-6 February 2006.

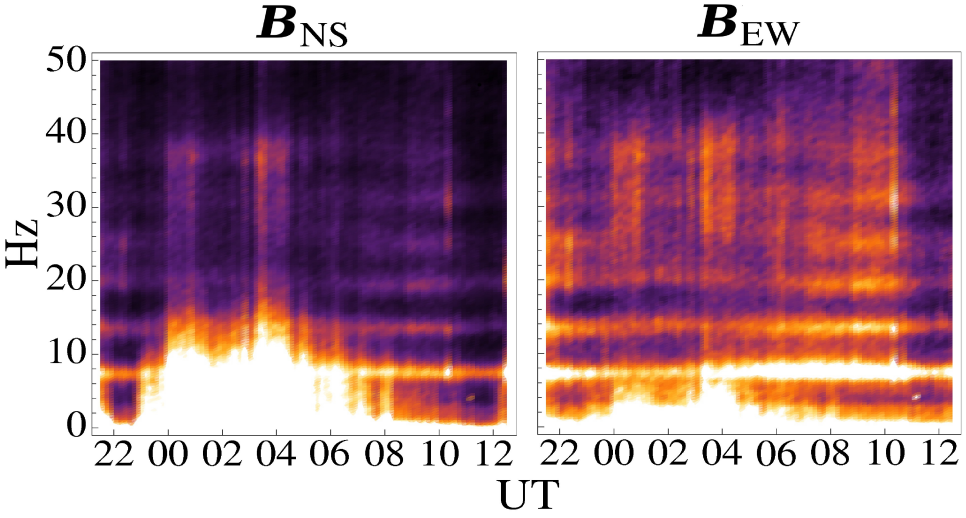

Spectrogram 14 hours long, Antarctica survey, 29-30 January 2008. The spectral resonance structures (SRS) can be observed.

Schumann resonance station in Sierra Nevada National Park

A SR measurement station designed by our team has been deployed in the National park of Sierra Nevada (Spain), at a height of 2500 m above the sea level.

Schumann resonance station: design and deployment

- Location: Sierra Nevada National Park (37º N, 3º 20' W), 2500 m above the sea level.
- Composed of two search coil magnetometers.
- Operative since the 18th July 2012.
- Very high sensitivity (1.9 mV/pt/Hz).
- SNR for 0.1 pT at 10 Hz: 16 dB.
- Bandwidth: 0.01 - 25 Hz.
- Supplied by solar panels/batteries. Data is automatically telemetered by means of GSM network.
- Time-series synchronized by GPS clock signal.

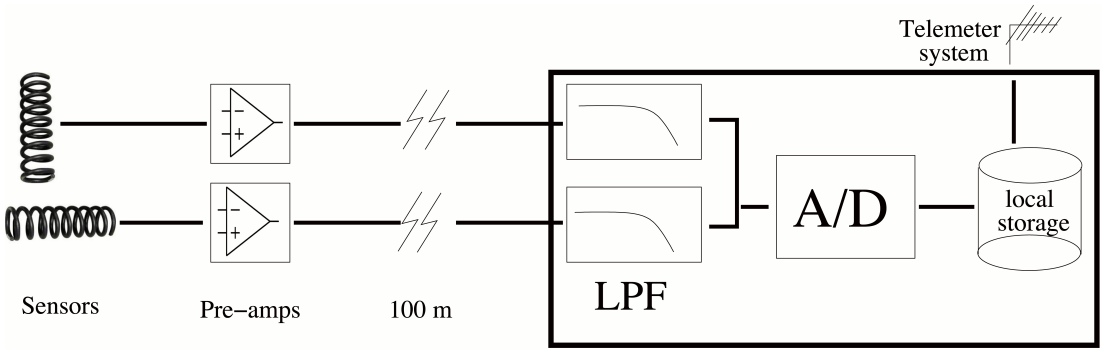

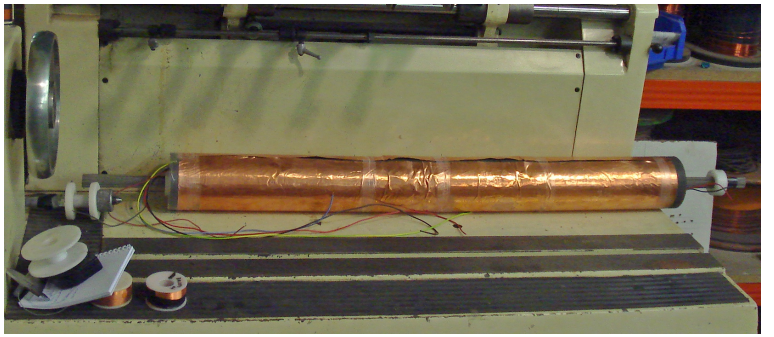

J. Fornieles, A. Salinas, S. Toledo-Redondo, A. Méndez, and J. Porti, Extremely Low Frequency Band Station for Natural Electromagnetic Noise Characterization, *IEEE Trans. Antennas Propag.*, submitted, 2013.

Schumann res. station, first results

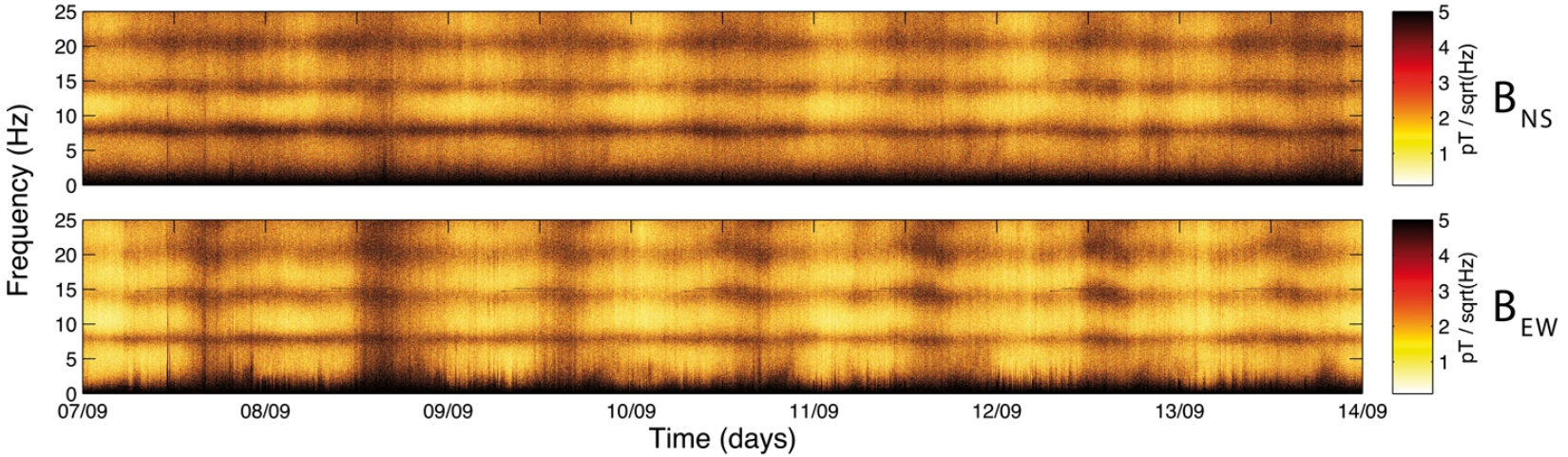

One week (7-14 September, 2012) spectrogram. Three SR can be observed.

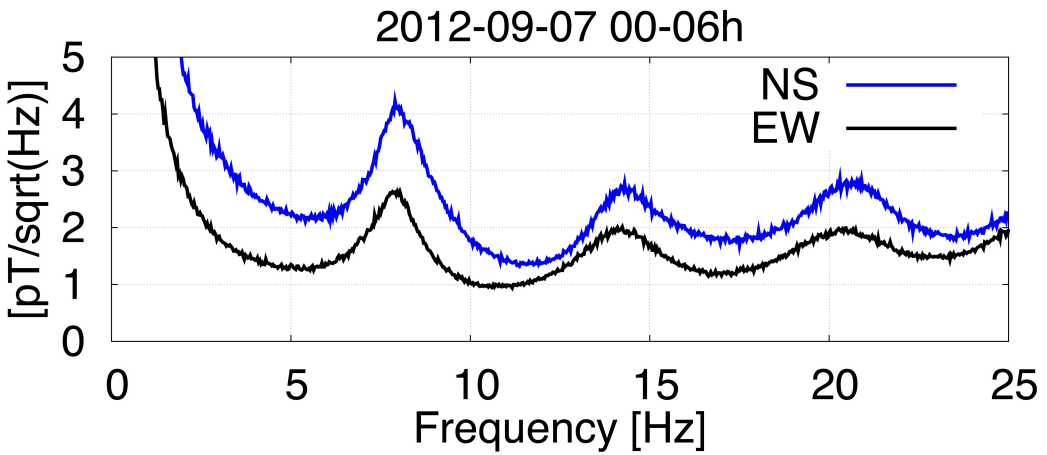

Calibrated *B* field spectrum of 6 hours length.

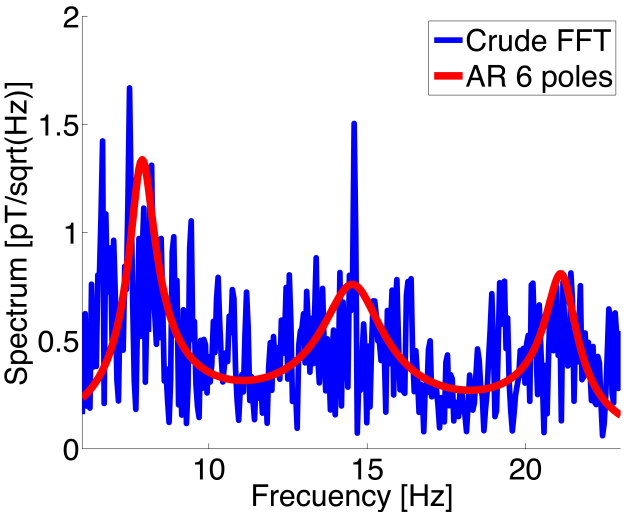

Autoregressive model for extraction of SR parameters.

Detection of Schumann resonances from space

The ”leaking” mechanism is not well understood.

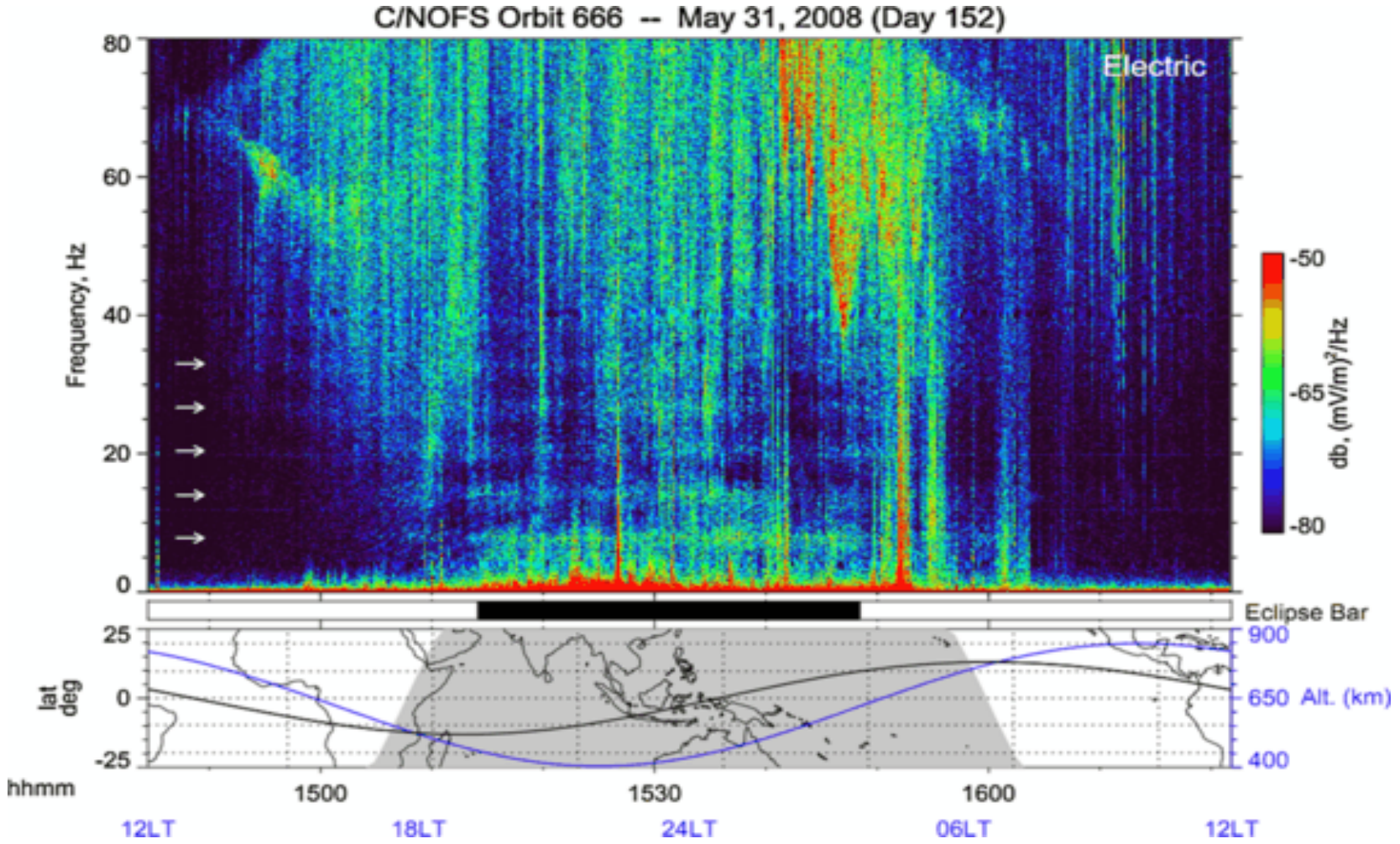

ELF measurements of C/NOFS satellite (700 km altitude, equatorial orbit). The Schumann resonances can be observed. Extracted from *Simoes et al.* [2011].

1st cut-off frequency detection from DEMETER

Electric field measurements from DEMETER detect the **cut-off frequency of the waveguide** as a minimum of energy.

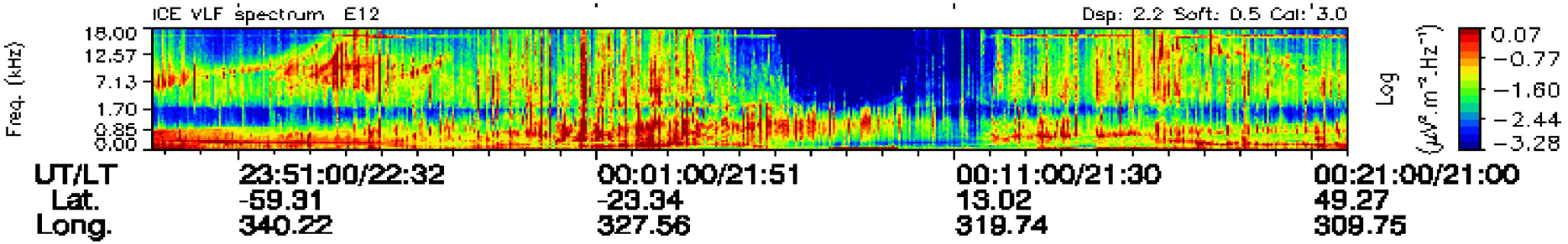

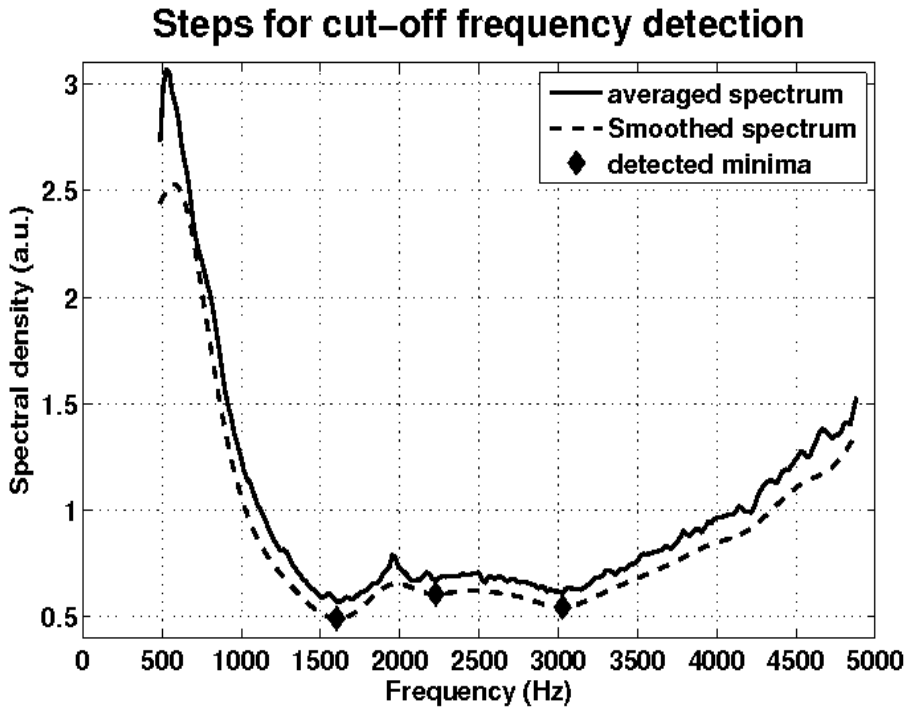

An algorithm was created to average the spectra of interest and automatically find the first cut-off frequency value (*fc*) for the corresponding group of spectra.

The **effective reflection height (*h*) of the ionosphere** can be deduced by means of the following formula, where *c* is the speed of light:

$$h = \frac{c}{2 f_c}$$

S. Toledo-Redondo, M. Parrot, and A. Salinas. Variation of the first cut-off frequency of the Earth-ionosphere waveguide observed by DEMETER, *J. Geophys. Res.*, vol. 117, pp. A04321, 2012.

Seasonal variation of the ionospheric height

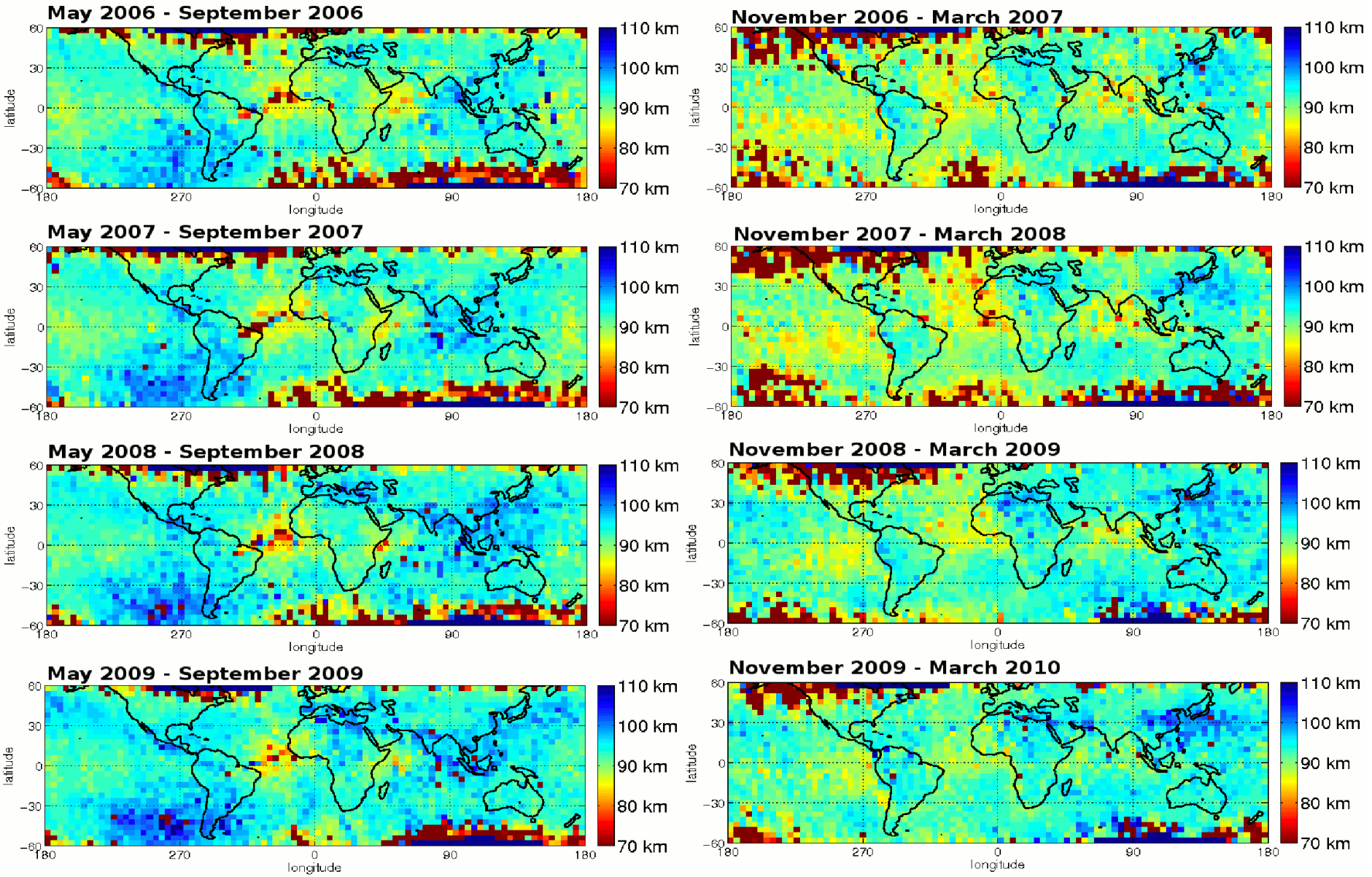

A **seasonal pattern** which repeats every year exists for the ionosphere height.

Other magnitudes which can be obtained

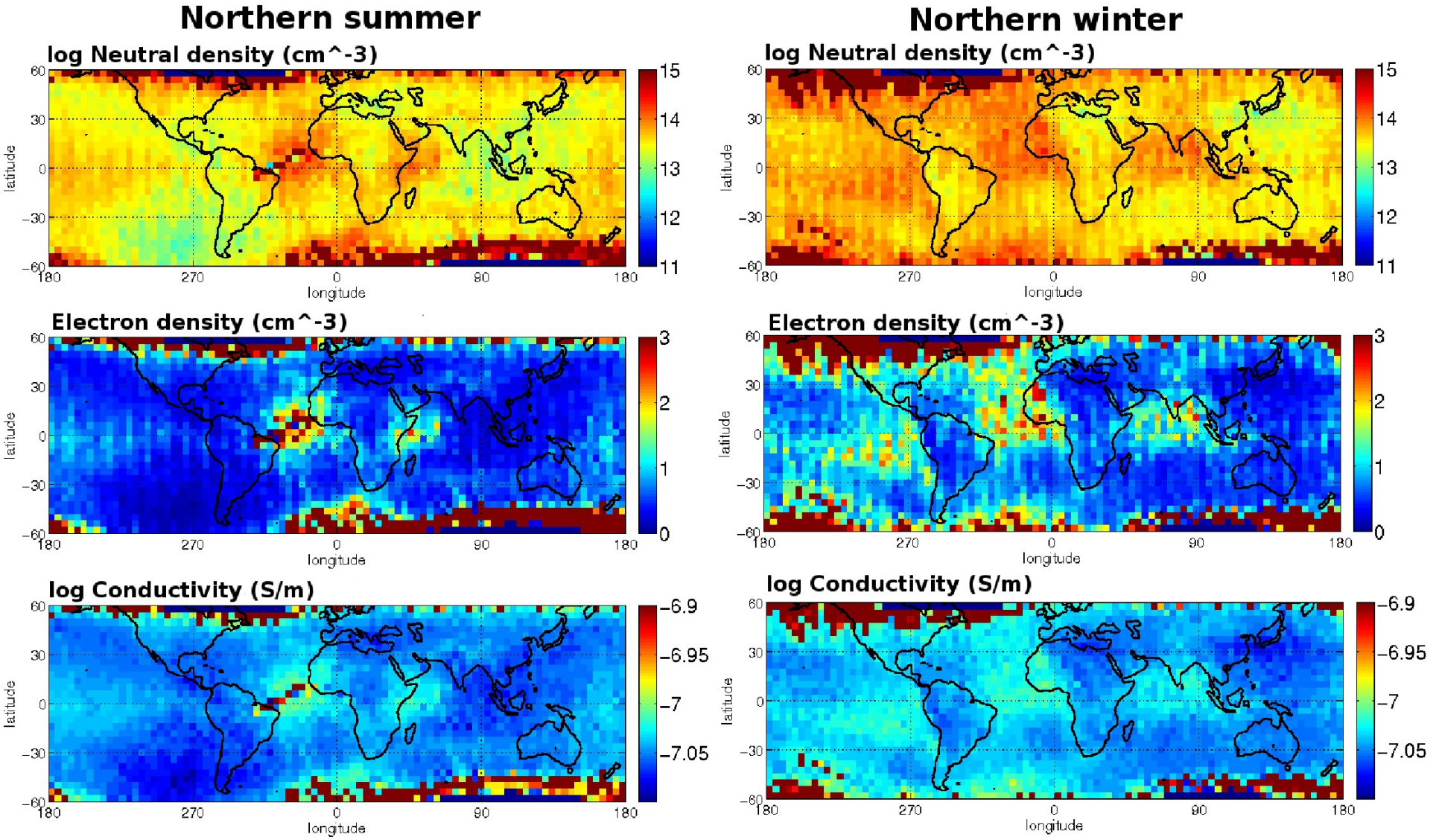

The **electron density** and **effective conductivity** at the reflection height can be calculated.

Cut-off frequency as a proxy of solar activity?

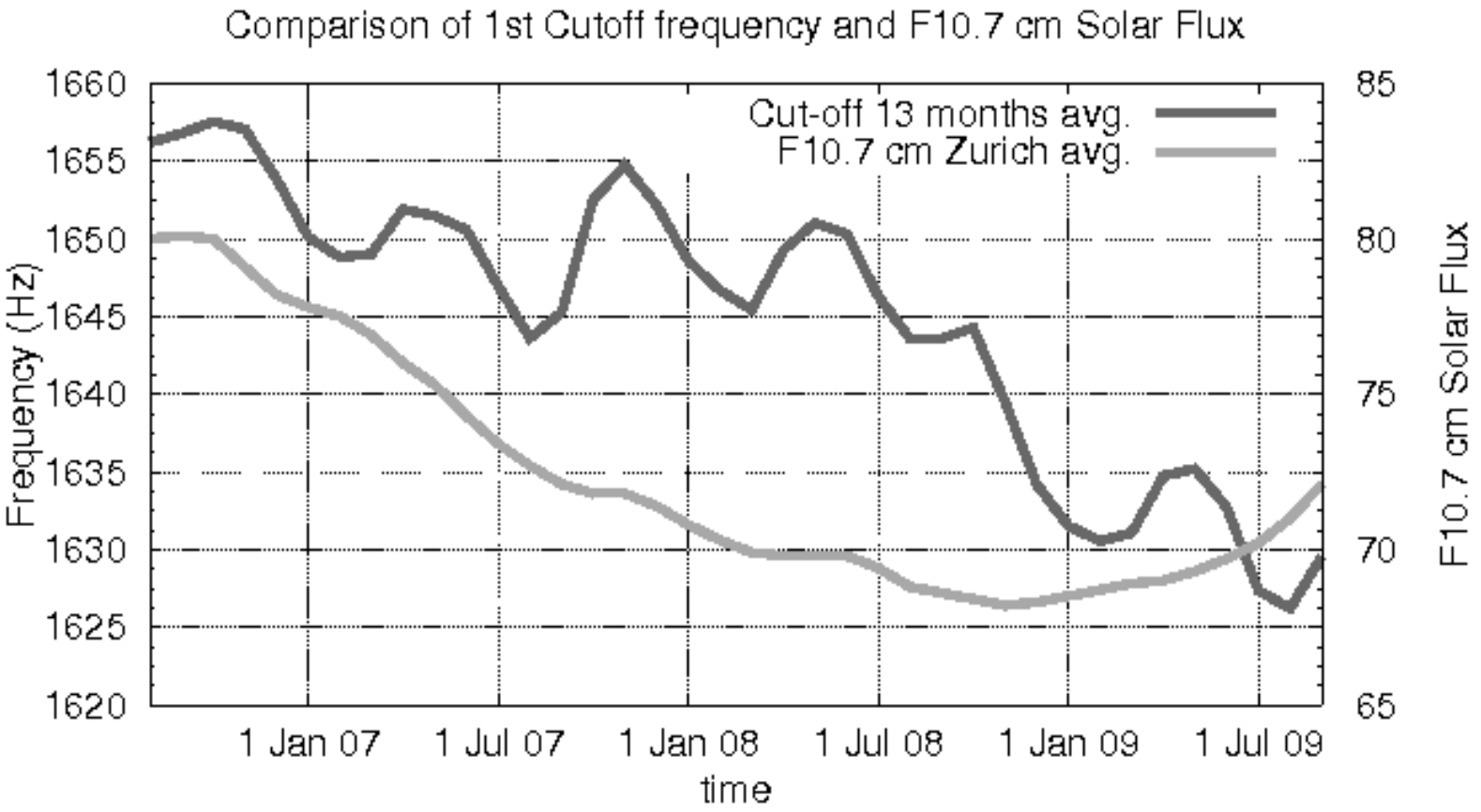

Comparison between **F10.7 cm solar flux parameter** and and the global **cut-off frequency** registered by DEMETER.

Present and future of Schumann resonances

- Schumann resonances are intimately **related to global thunderstorm activity**, and therefore to tropospheric climate. They can be a tool for studying the climate.

- Schumann resonances can be also employed to study / monitor **changes in the lower ionosphere**, like for instance the day-night asymmetry, solar storms or nuclear explosions.

- Schumann resonances have also interest for the **study of other celestial bodies**. Its existence implies electric activity in the atmosphere of the planet / moon.

- Schumann resonances have been proposed as a tool for **earthquake prediction.** However, the physical mechanisms involved are not clear and the observations are **not fully conclusive**.

- **Analytical treatment** of the Earth-ionosphere cavity becomes unfeasible except for very strong simplified models.

- **Numerical models** of the Earth-ionosphere cavity are complex due to the different sizes involved (100 km height, 6400 km radius).

- The ramdom behavior of lightning makes difficult to interpret SR **observations**. Improvements in the uderstanding global lightning activity are required.

THANK YOU !

Disturbance generated by an earthquake

- The studied disturbances consist of **local variations in the atmospheric conductivity**.
- The disturbance follows a gaussian distribution in the space, its maximum being at the **epicenter** of the earthquake.
- The total radius of the disturbance is determined by the earthquake magnitude ($r = 10^{0.43M}$) (1).
- Different degrees of disturbances are proposed, based on the idea of forcing down the conductivity profile (***h* = 5, 10, 20, 40 km**) (2).

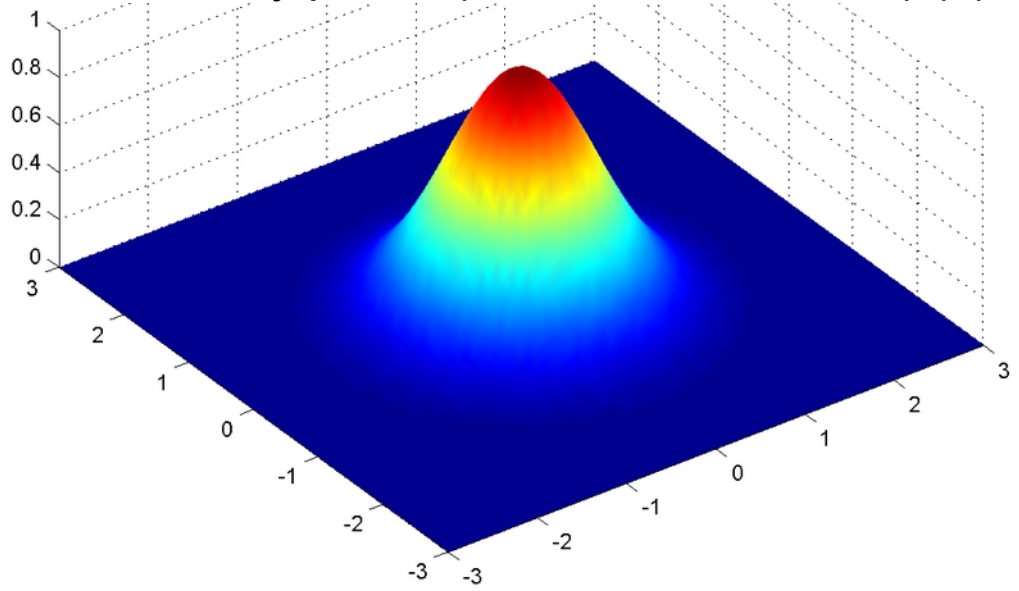

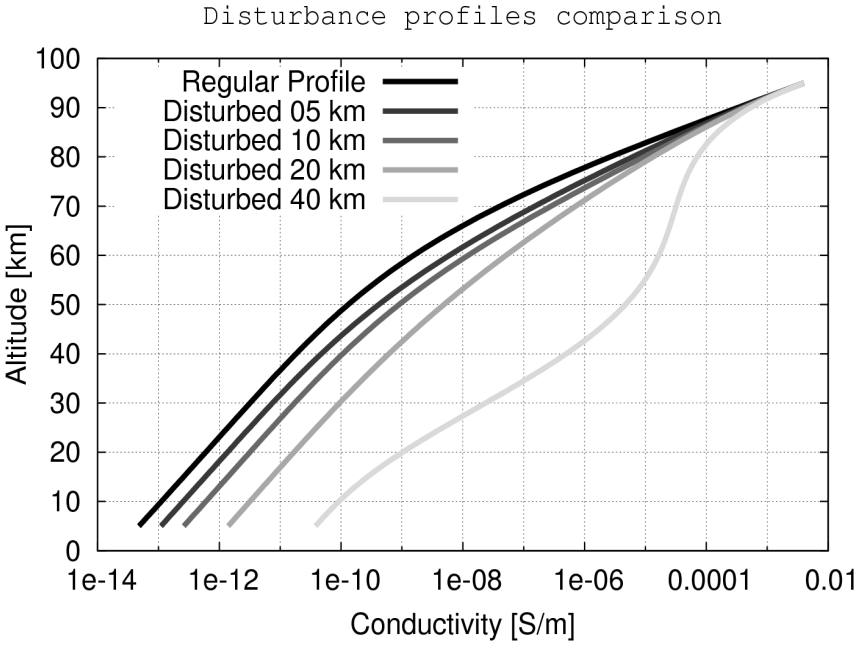

(1) S. Pulinets and K. Boyarchuk, *Ionospheric precursors of earthquakes*, pp. 16, Springer- Verlag Berlin, Germany, 2004.
(2) A.P. Nickolaenko et al., Model modifications in Schumann resonance intensity caused by a localized ionosphere over the earthquake epicenter, *Annales Geophysicae*, 24, 567-575, 2006.

The DEMETER micro-satellite

DEMETER (Detection of Electro-Magnetic Emissions Transmitted from Earthquake regions) is a french **micro-satellite** which carries several instruments for the **study of earthquake precursors**.

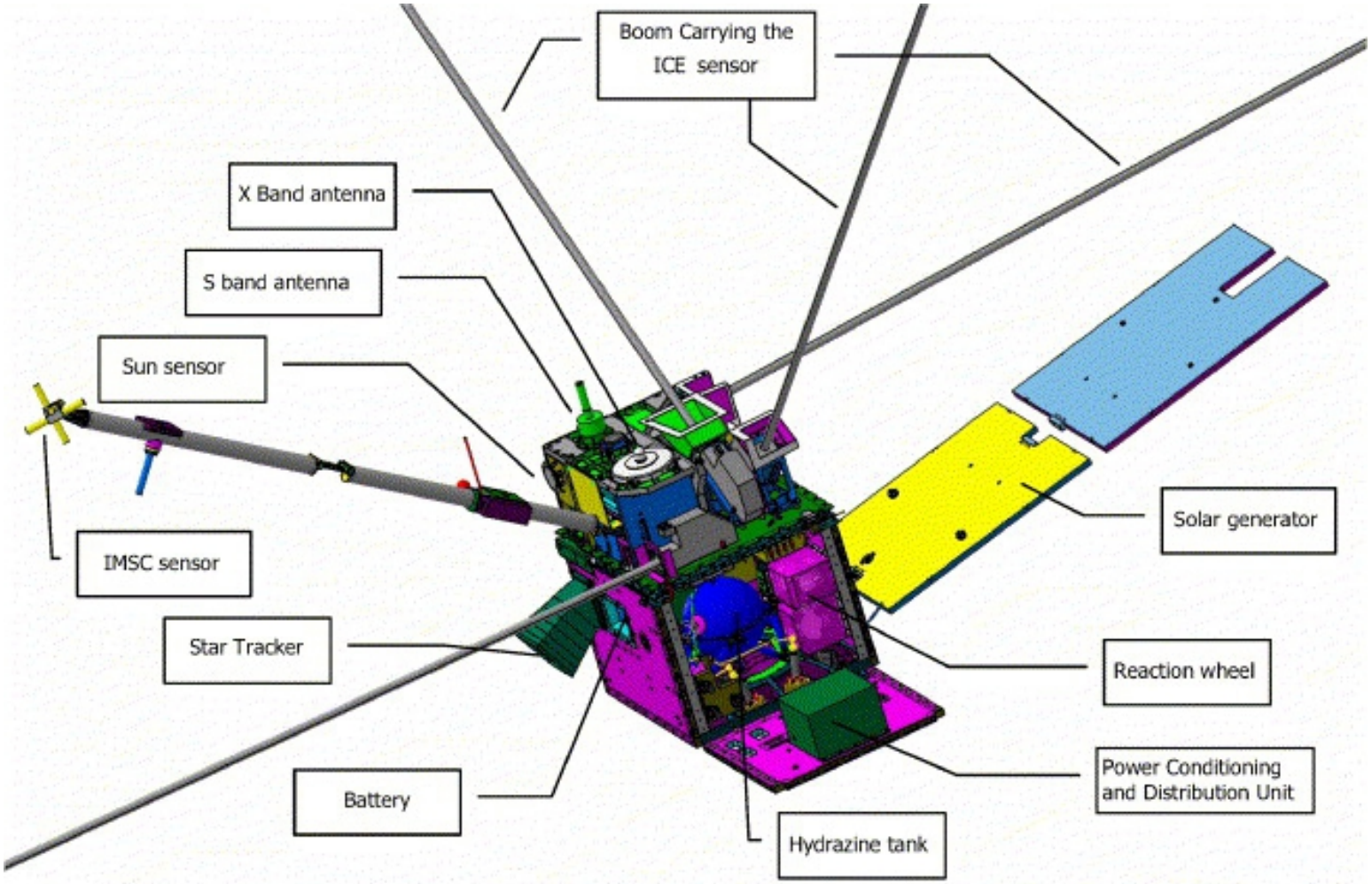

M. Parrot, Special Issue of planetary and space science ”DEMETER”, *Planet. Space Sci.*, vol. 54, pp. 411-412, 2006

Monthly variation of the ionosphere height

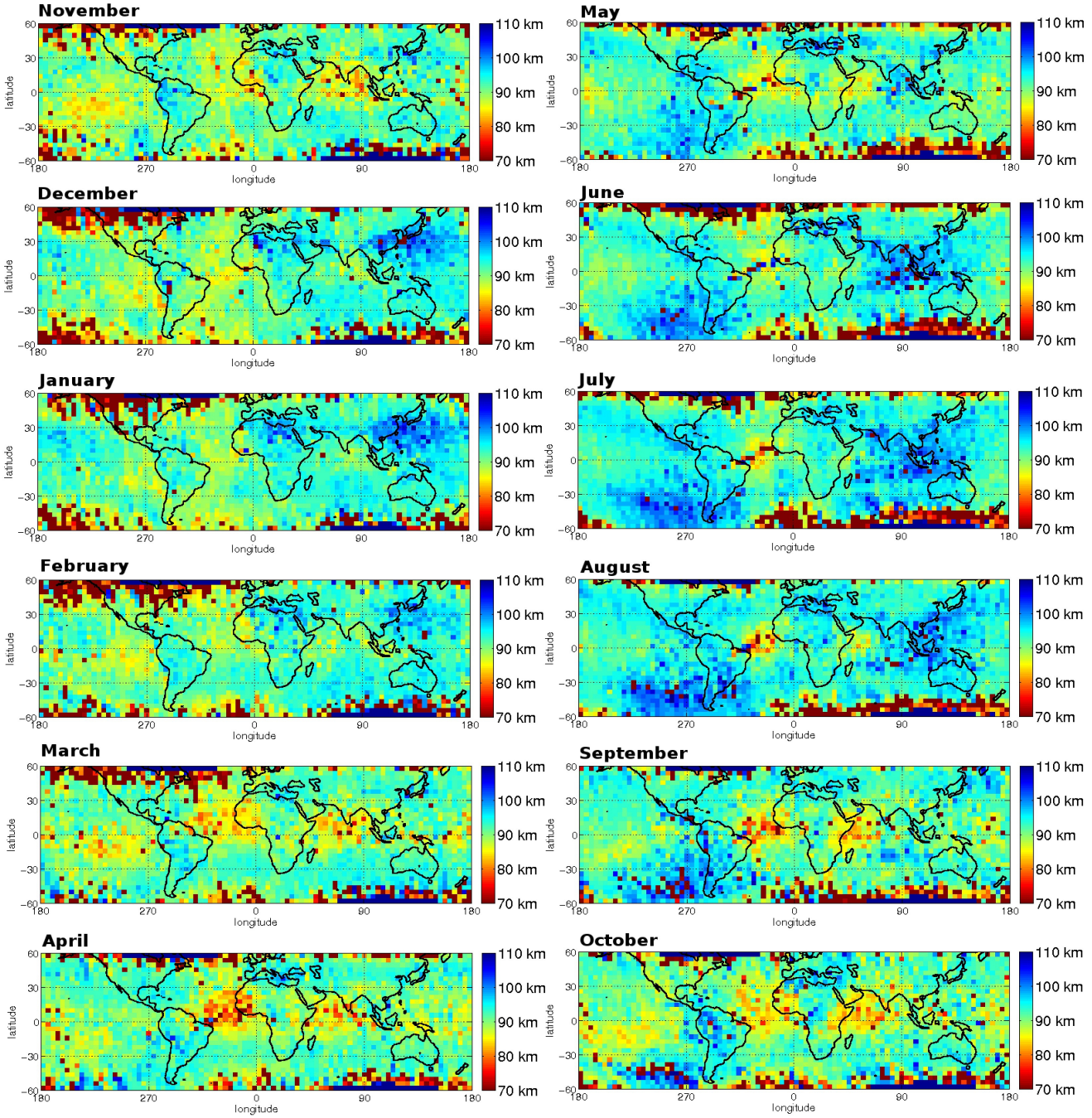

Data from 4 years (2006 - 2009) was employed for this study. Here we see the effective ionospheric reflection height for the averaged months during all the time span.

Seasonal change on 1st cut-off frequency

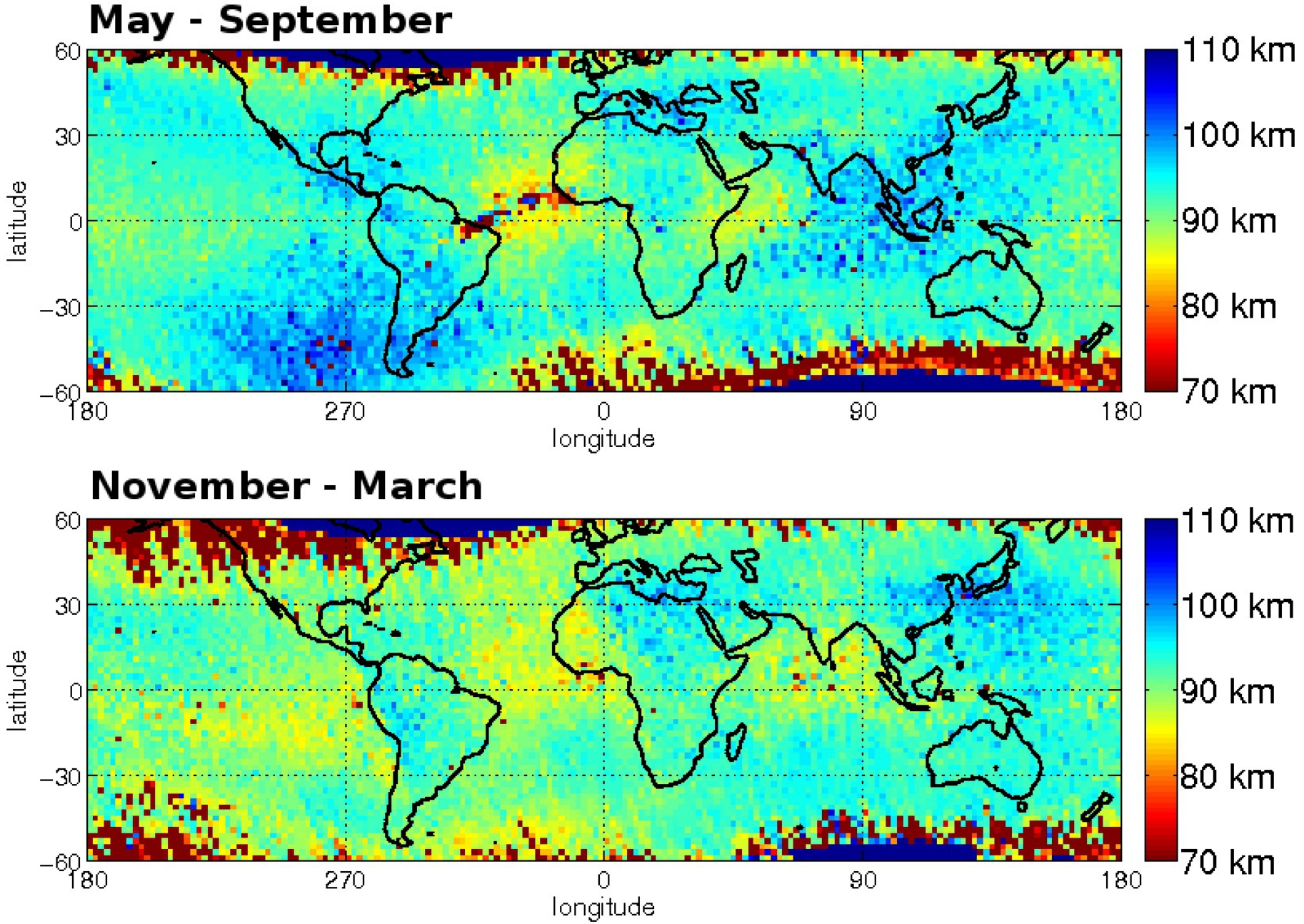

Effective height from IRI + MSIS

Map of the effective reflection height at 22.30 LT, calculated with IRI + MSIS models.

The variations are much smaller than the ones measured from DEMETER.

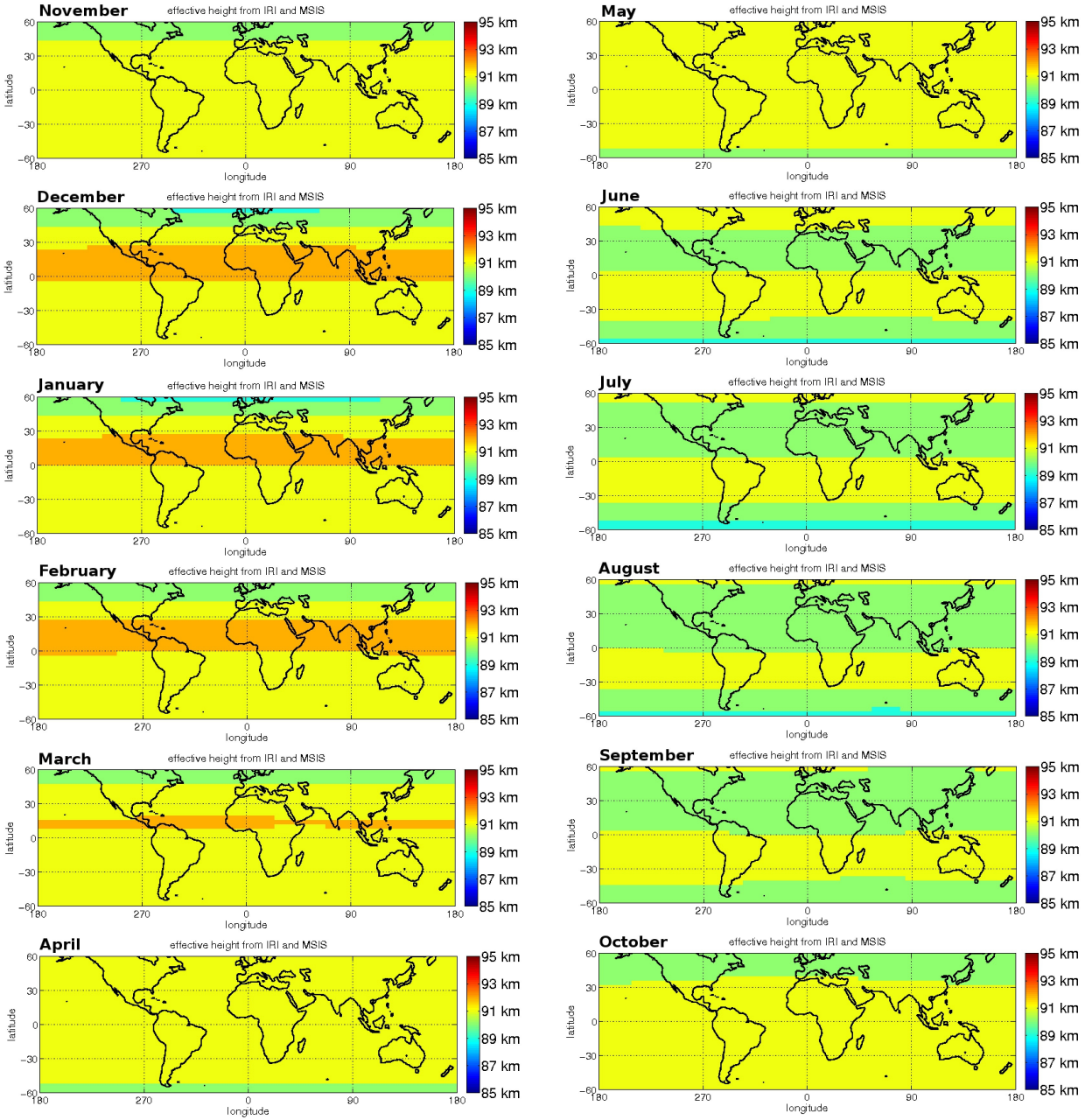

Modeling atmospherics

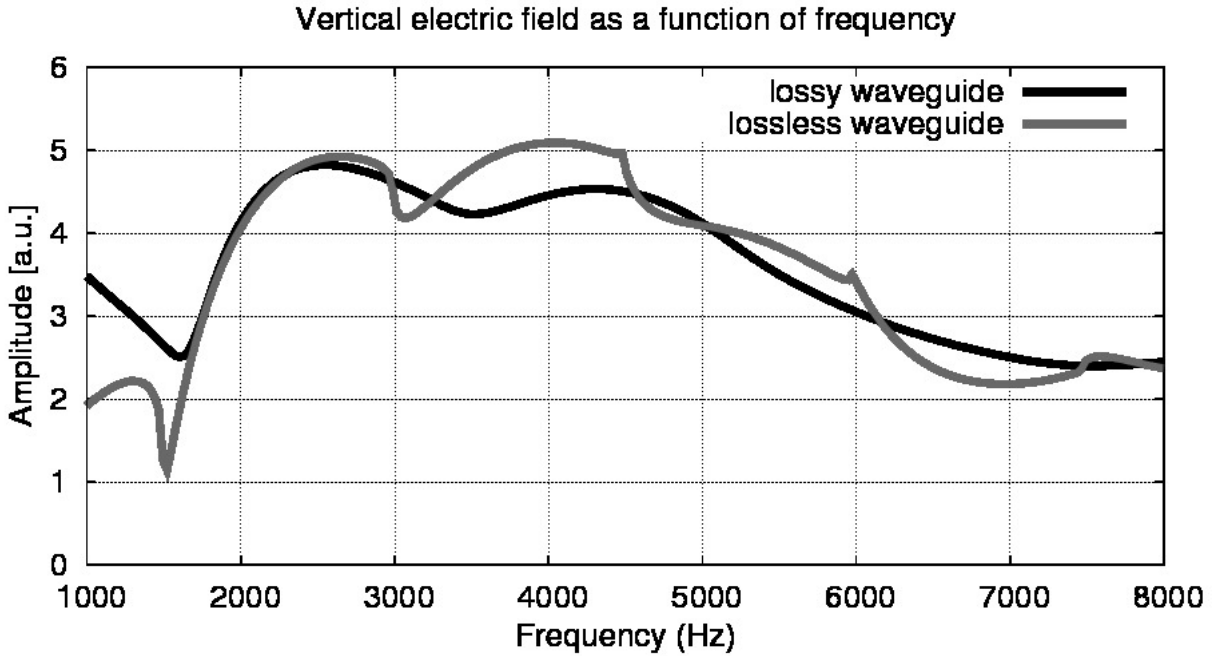

Cut-off frequency for lossless and lossy waveguides.

Effect of Round Robin memory allocation policy.